Physics and Astronomy Faculty Publications and Presentations

College of Sciences

8-10-2014

The green bank northern celestial cap pulsar survey. I. survey description data analysis and initial results

K. Stovall

R. S. Lynch

S. M. Ransom

A. M. Archibald

S. Banaszak

See next page for additional authors

Recommended Citation

Authors

K. Stovall, R. S. Lynch, S. M. Ransom, A. M. Archibald, S. Banaszak, C. M. Biwer, J. Boyles, L. P. Dartez, D. Day, A. J. Ford, J. Flanigan, A. Garcia, J. W.T. Hessels, J. Hinojosa, F. A. Jenet, D. L. Kaplan, C. Karako-Argaman, V. M. Kaspi, V. I. Kondratiev, S. Leake, D. R. Lorimer, G. Lunsford, J. G. Martinez, A. Mata, M. A. McLaughlin, M. S.E. Roberts, M. D. Rohr, X. Siemens, I. H. Stairs, and J. Van Leeuwen

THE GREEN BANK NORTHERN CELESTIAL CAP PULSAR SURVEY. I. SURVEY DESCRIPTION, DATA ANALYSIS, AND INITIAL RESULTS

K. Stovall[1,2,3], R. S. Lynch[4], S. M. Ransom[5], A. M. Archibald[4,6], S. Banaszak[7], C. M. Biwer[7,8], J. Boyles[9],
L. P. Dartez[1], D. Day[7], A. J. Ford[1], J. Flanigan[7], A. Garcia[1], J. W. T. Hessels[6,10], J. Hinojosa[1], F. A. Jenet[1],
D. L. Kaplan[7,11], C. Karako-Argaman[4], V. M. Kaspi[4], V. I. Kondratiev[6,12], S. Leake[1], D. R. Lorimer[13], G. Lunsford[1],
J. G. Martinez[1], A. Mata[1], M. A. McLaughlin[13], M. S. E. Roberts[14], M. D. Rohr[7], X. Siemens[7], I. H. Stairs[15],
J. van Leeuwen[6], A. N. Walker[7], AND B. L. Wells[7,16]

[1] Center for Advanced Radio Astronomy, University of Texas at Brownsville, One West University Boulevard,
Brownsville, TX 78520, USA; stovall.kevin@gmail.com
[2] Department of Physics and Astronomy, University of Texas at San Antonio, San Antonio, TX, USA
[3] Department of Physics and Astronomy, University of New Mexico, Albuquerque, NM, USA
[4] Department of Physics, McGill University, 3600 University Street, Montreal, QC H3A 2T8, Canada
[5] National Radio Astronomy Observatory, 520 Edgemont Road, Charlottesville, VA 22901, USA
[6] ASTRON, the Netherlands Institute for Radio Astronomy, Postbus 2, 7990 AA Dwingeloo, The Netherlands
[7] Physics Department, University of Wisconsin–Milwaukee, Milwaukee, WI 53211, USA
[8] Department of Physics, Syracuse University, Syracuse, NY 13244, USA
[9] Department of Physics and Astronomy, Western Kentucky University, Bowling Green, KY 42101, USA
[10] Astronomical Institute "Anton Pannekoek," University of Amsterdam, Postbus 94249, 1090 GE Amsterdam, The Netherlands
[11] Department of Astronomy, University of Wisconsin–Madison, 475 North Charter Street, Madison, WI 53706-1582, USA
[12] Space Center of the Lebedev Physical Institute, Profsoyuznaya str. 84/32, Moscow 117997, Russia
[13] Department of Physics, West Virginia University, 210E Hodges Hall, Morgantown, WV 26506, USA
[14] Eureka Scientific, Inc., 2452 Delmer Street, Suite 100, Oakland, CA 94602-3017, USA
[15] Department of Physics and Astronomy, University of British Columbia, 6224 Agricultural Road, Vancouver, BC V6T 1Z1, Canada
[16] Department of Atmospheric Science, Colorado State University, Fort Collins, CO, USA

ABSTRACT

We describe an ongoing search for pulsars and dispersed pulses of radio emission, such as those from rotating radio transients (RRATs) and fast radio bursts, at 350 MHz using the Green Bank Telescope. With the Green Bank Ultimate Pulsar Processing Instrument, we record 100 MHz of bandwidth divided into 4096 channels every $81.92\,\mu$s. This survey will cover the entire sky visible to the Green Bank Telescope ($\delta > -40°$, or 82% of the sky) and outside of the Galactic Plane will be sensitive enough to detect slow pulsars and low dispersion measure ($<30\,\mathrm{pc\,cm^{-3}}$) millisecond pulsars (MSPs) with a 0.08 duty cycle down to 1.1 mJy. For pulsars with a spectral index of -1.6, we will be 2.5 times more sensitive than previous and ongoing surveys over much of our survey region. Here we describe the survey, the data analysis pipeline, initial discovery parameters for 62 pulsars, and timing solutions for 5 new pulsars. PSR J0214+5222 is an MSP in a long-period (512 days) orbit and has an optical counterpart identified in archival data. PSR J0636+5129 is an MSP in a very short-period (96 minutes) orbit with a very low mass companion (8 M_J). PSR J0645+5158 is an isolated MSP with a timing residual RMS of 500 ns and has been added to pulsar timing array experiments. PSR J1434+7257 is an isolated, intermediate-period pulsar that has been partially recycled. PSR J1816+4510 is an eclipsing MSP in a short-period orbit (8.7 hr) and may have recently completed its spin-up phase.

Key words: binaries: close – binaries: eclipsing – binaries: general – pulsars: general – pulsars: individual – surveys

Online-only material: color figures

1. INTRODUCTION

Since their initial discovery over 45 yr ago (Hewish et al. 1968), radio pulsars have been excellent laboratories for a wide range of physics. They have provided some of the most stringent tests of general relativity (Taylor & Weisberg 1989; Kramer et al. 2006), as well as alternative theories of gravity (Freire et al. 2012). Some pulsars have been identified as laboratories for extreme physics due to their strong magnetic fields (Gavriil et al. 2008) or exceptionally large densities (Demorest et al. 2010; Antoniadis et al. 2013). Pulsars are important probes of the Galactic neutron star population; those in binary (or multi-body) systems also provide probes of their companion(s), which can be, e.g., planets (Wolszczan & Frail 1992), a white dwarf (e.g., van Kerkwijk et al. 2005), a main sequence star (Johnston et al. 1992; Kaspi et al. 1994), another neutron star (Hulse & Taylor 1975), or even another pulsar (Burgay et al. 2003).

Despite the discovery of over 2300 pulsars, pulsar searches are still uncovering novel systems, including extremely fast-spinning millisecond pulsars (MSPs; Hessels et al. 2006), MSPs in orbit with main sequence star companions (Champion et al. 2008), a very dense planetary mass companion (Bailes et al. 2011), pulsars that appear to be transitionary objects from low mass X-ray binaries to MSPs (Archibald et al. 2009; Kaplan et al. 2012; Papitto et al. 2013), and a hierarchical stellar triple system (Ransom et al. 2014).

Radio pulsars, particularly MSPs, are excellent clocks spread throughout our galaxy. In recent years, there has been a strong effort to use an ensemble of MSPs, known as a pulsar timing array (PTA), for direct gravitational wave (GW; van Haasteren et al. 2011; Manchester et al. 2013; Demorest et al. 2013) detection. Currently, there are four PTA experiments ongoing, including the North American Nanohertz Observatory for Gravitational Waves (NANOGrav), the Parkes Pulsar Timing
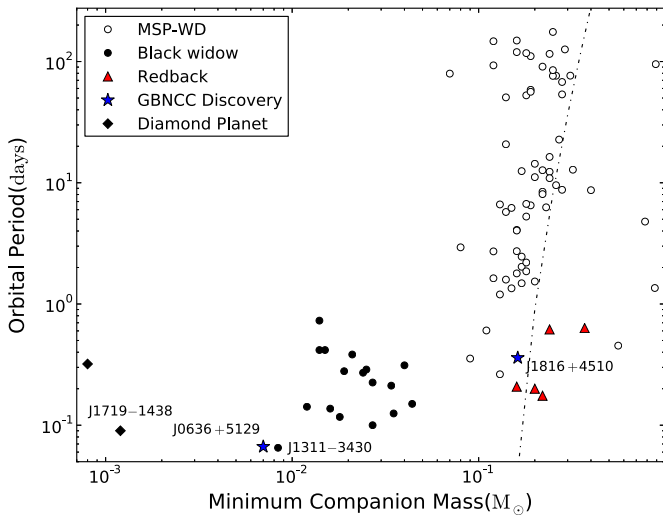
Figure 1. Minimum companion mass vs. orbital period for Galactic field MSPs ($P < 10$ ms). Pulsars from the ATNF pulsar catalog are shown as unfilled black circles, known redbacks are filled red circles, known black widows are filled black circles, PSR J1719−1438 and another similar system described in Ng (2013) are shown as black diamonds; and our discoveries are marked with blue stars. Parameters for redback and black widow pulsars were taken from Roberts (2011) and M. S. E. Roberts (2014, private communication). The dashed line shows the relation between companion mass and orbital period given by Tauris & Savonije (1999).

(A color version of this figure is available in the online journal.)

Array, the European Pulsar Timing Array, and a combination of these three known as the International Pulsar Timing Array. A successful detection of GWs by a PTA will require a large number (20–40) of MSPs spread across the sky, each of which must be timed with enough precision to predict its pulse times-of-arrival to within tens to hundreds of nanoseconds. Recent pulsar surveys have shown that we're still far from having found all of the best pulsar clocks in the Galaxy; thus pulsar surveys are an important component in the effort to directly detect nano-Hertz gravitational waves. Discovering MSPs that are suitable for PTAs is the primary driver for the survey we present here.

Two complementary search strategies are employed to discover new pulsars. One is through targeted searches of specific objects including supernova remnants (for a review, see Camilo 2003), globular clusters (Manchester et al. 1991; Biggs et al. 1994; D'Amico et al. 2001; Ransom et al. 2005; Hessels et al. 2007), or high-energy counterparts, such as gamma-ray point sources identified by the *Fermi Gamma-Ray Space Telescope* (e.g., Hessels et al. 2011; Ransom et al. 2011; Keith et al. 2011; Kerr et al. 2012). Such targeted searches can be highly efficient, however they are biased to what type of pulsar they can discover. Searches of globular clusters yield large numbers of MSPs, but timing effects due to motion induced by the potential of the globular cluster and stars near the MSP are difficult to distinguish from the timing effects expected to be caused by GWs. Also, MSPs discovered in globular clusters are typically very distant and therefore weak and strongly affected by propagation through the ionized interstellar medium. *Fermi*-identified point sources that are revealed to be pulsars are often MSPs (at least off the Galactic plane), but in a large fraction of these systems the companion is being ablated by the MSP. These systems often exhibit eclipses for a significant fraction of the orbital period and have orbital effects that are detrimental to their use in GW detection. Though there are certainly some *Fermi*-discovered

MSPs that are promising for PTAs (e.g., PSR J2043+1711; Guillemot et al. 2012), there are also many important PTA sources that have no *Fermi* counterpart. The other approach to pulsar searches involves more shallow surveys of large areas of sky. Such surveys complement the targeted searches by discovering nearby sources (ideal for multi-wavelength follow up and often good for PTAs) and filling out the total population.

Over the last five or so years, many new members of two related binary pulsar populations have been discovered. One population was first recognized with the discovery of the so-called "black widow" system (B1957 + 20; Fruchter et al. 1988). It was called the black widow system due to evidence that the companion is being ablated by the pulsar's wind. Roughly a dozen systems with similar characteristics, including eclipses of the pulsar or DM variations of the pulsar's signal near superior conjunction, orbital periods ranging from about 1.5 to 30 hr, and very-low-mass ($M \sim 0.01$–$0.05\,M_\odot$) companions have been discovered since. Pulsar systems with similar characteristics to the black widow systems, but with low to moderate mass companions ($M \sim 0.15$–$0.7\,M_\odot$), have also been discovered (e.g., Archibald et al. 2009). Given the similarities between these and the black widow systems, they are often referred to as "redback" systems (Roberts 2011).

Another recently discovered population, the "diamond planet" systems, currently only contains two samples, J1719−1438 (Bailes et al. 2011) and another system described in Ng (2013). The J1719−1438 system contains a planetary mass companion ($1.2\,M_J$) in a very tight orbit ($P_{\rm orb} = 2.2$ hr). It is believed that these systems resulted from an ultracompact X-ray binary system in which the companion narrowly avoided being completely destroyed. We introduce these populations here since we will describe newly discovered sources in Section 6 that may be members of these populations. A plot showing the relationship among typical binary pulsars with white dwarf companions, the black widow population, the redback population and the diamond planet system are shown in Figure 1.

Driven by discovering exotic pulsar systems and the need for many more PTA-worthy pulsars at a variety of angular separations from one another, there are several large-scale pulsar surveys currently underway. Here we describe the Green Bank Northern Celestial Cap (GBNCC) survey. The GBNCC will survey the entire sky visible to the Robert C. Byrd Green Bank Radio Telescope (GBT) at 350 MHz for radio pulsars and fast radio transients. As of 2014 March 18, we have discovered 67 new radio pulsars,[17] including 9 MSPs ($P < 10$ ms) and 6 intermediate-spin-period pulsars (10 ms $< P < 100$ ms) after completing the processing of 20% of the entire survey. We have also discovered an additional seven rotating radio transients[18] (RRATs), which will be presented in subsequent papers. In Section 2, we give a detailed description of the survey, followed by a description of the data analysis and candidate rating in Section 3. Section 4 lists re-detections of previously known pulsars, which we use to estimate the sensitivity of our survey and provide for calibrating population simulations. Section 5 describes the procedure we are using to follow-up our discovered pulsars. In Section 6, we present results for 67 discovered pulsars; we give discovery parameters for 62 pulsars and timing solutions for 5 of our first discoveries. We are currently following up the five pulsars presented here and

---

[17] For an up-to-date total, see http://arcc.phys.utb.edu/gbncc/.
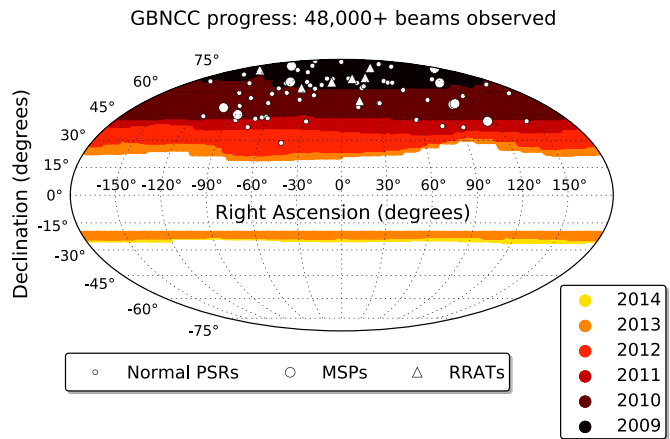[18] As of 2014 March 18, see footnote 17 to get an up-to-date total.

Figure 2. Sky covered to date by the GBNCC survey. Colors indicate our coverage for each year from 2009 to 2014. Our discoveries are also shown; small dots indicate normal pulsars, large circles correspond to MSPs, and triangles indicate RRATs.

(A color version of this figure is available in the online journal.)

our other discoveries (including the RRATs) using the GBT and the Low Frequency Array (LOFAR; van Haarlem et al. 2013; Stappers et al. 2011).

2. SURVEY DESCRIPTION

After the success of the GBT 350 MHz Drift Scan survey (GBT350; Boyles et al. 2013; Lynch et al. 2013) as well as with the installation of the new Green Bank Ultimate Pulsar Processor[19] (GUPPI) backend, we developed a plan to perform an all-sky pulsar survey, known as the GBNCC survey, using the GBT at 350 MHz. The GBNCC survey uses the GUPPI backend, which provides increased bandwidth and time resolution over the Spigot (Kaplan et al. 2005) backend used by the GBT350 survey. The GBNCC survey is divided into two stages: the first, which has been completed, covered the entire sky north of $\delta = 38°$, and the second, which covers the remaining GBT visible sky, is currently being carried out. The positions of our pointings were calculated from a generalized spiral set beginning at the North Pole as described in Saff & Kuijlaars (1997) using the Golden Section as the angle between successive points for a set containing 152,000 points. The number of points used to cover the celestial sphere were chosen so that the HWHM (18′) for the GBT's 350 MHz reciever would overlap with adjacent pointings by about 10% to provide good coverage of the entire sky. Each pointing consists of a 120 s integration on a particular sky location, with data recorded from 300 to 400 MHz divided into 4096 frequency channels. The vast majority of our pointings were recorded with a sample time of 81.92 μs, but there were 207 pointings (all close to the northern celestial pole) taken during the first few days of the survey with a sample time of 163.84 μs. Stage I of this survey was performed from 2009 October 23 to 2011 October 17 and resulted in $\approx$30,000 sky pointings. The data resulting from these pointings are still undergoing data processing. We have processed about 80% of these pointings and roughly 20% of these candidates have been looked at by human eye. We have begun the second stage and as of 2013 March 18 have covered about 40% (13,500 deg^2) of the GBT visible sky. Figure 2 shows our survey progress from 2009 until now.

The theoretical minimum detectable flux density for a pulsar survey is given by

$$S_{\min} = \frac{(S/N_{\min}) T_{\text{sys}}}{G \sqrt{n_p t_{\text{int}} \Delta f}} \sqrt{\frac{W}{P - W}}, \qquad (1)$$

where $S/N_{\min}$ is the minimum signal-to-noise ratio (S/N) required to detect a source, T_{sys} is the system temperature in K, G is the telescope gain in K Jy^{-1}, n_p is the number of polarizations summed, t_{int} is the integration time in s, Δf is the bandwidth in MHz, W is the width of the pulse as detected by the system in s, and P is the pulsar's period in s (Dewey et al. 1985). In our sensitivity estimates, we used $S/N_{\min}$ values of either 12 or 15 to adjust for sensitivity differences of surveys due to analog to digital conversion losses. We used a value of 12 for currently ongoing surveys that use multi-bit systems and we used 15 for past surveys. The values of 12 and 15 are conservative and account for sensitivity reduction due to radio frequency interference (RFI). We note that although we use an S/N of 12 for the estimated sensitivity of our survey, in the data analysis described in Section 3, we fold candidate pulsars down to a significance of 6 (the lowest S/N of a pulsar blindly detected to date is about 8.5). The GBT has a gain of about 2 K Jy^{-1} at 350 MHz. The total system temperature is the receiver temperature (T_{rec}) plus the sky temperature (T_{sky}). The receiver temperature at 350 MHz for the GBT is about 23 K. The sky temperature is highly dependent on sky position and observing frequency due to Galactic synchrotron emission. Since we are estimating sensitivities for a large area of sky, we use the average sky temperature of 34.4 K at 408 MHz (Haslam et al. 1982) and calculate an estimate for T_{sky} at 350 MHz using the spectral index -2.6 (Haslam et al. 1982). For the GBNCC survey, we use $\Delta f = 80$ MHz to adjust for rolloff on the edge of the 100 MHz band, $t_{\text{int}} = 120$ s, and $n_p = 2$. The pulse width (W) is not just a function of the pulsar, but also of incorrected pulse broadening due to propagation through the interstellar medium. Dispersion in the interstellar medium widens the pulse as

$$\tau_{\text{DM}} \approx 8.3 \, \mu s \times \left(\frac{\Delta f}{\text{MHz}} \right) \times \left(\frac{f}{\text{GHz}} \right)^{-3} \times \left(\frac{\text{DM}}{\text{pc cm}^{-3}} \right), \quad (2)$$

where f is the center frequency of a frequency channel and Δf is the channel bandwidth. To minimize dispersive pulse broadening, we use 4096 frequency channels across the observing bandwidth. For dispersion measure (DM) = 100 pc cm^{-3}, our setup would result in a dispersive pulse smearing of 0.5 ms. Another effect of the interstellar medium is scattering, which broadens the pulse roughly according to

$$\log \left(\frac{\tau_{\text{scatt}}}{\mu s} \right) = -3.59 + 0.129 \log (\text{DM}) + 1.02 \log (\text{DM})^2$$
$$- 4.4 \log \left(\frac{f}{\text{GHz}} \right) \qquad (3)$$

(Cordes 2002). Since we are unable to mitigate the effect of scattering, it is difficult to detect most MSPs beyond a DM of 100 pc cm^{-3} ($\tau_{\text{scatt}} \sim 0.8$ ms) at these frequencies. We note that though the dispersion law in Equation (2) is very accurate, the scattering relation in Equation (3) is highly uncertain and the scattering for some lines-of-sight can vary from this relation by over an order of magnitude. Scattering, combined with higher sky temperature, makes the GBNCC survey less sensitive to distant pulsars in the Galactic plane,
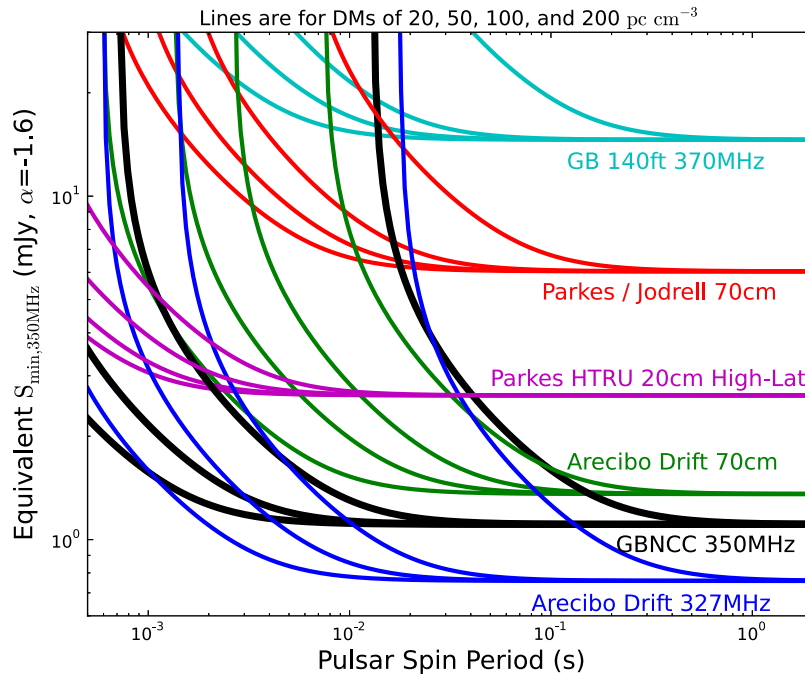
Figure 3. Estimated sensitivity of the GBNCC survey compared to the estimated sensitivities of five other pulsar surveys. For each survey, sensitivities are calculated using DMs of 20, 50, 100, and 200 pc cm^{-3}. In each case, the DM = 20 pc cm^{-3} curve is the leftmost and the DM = 200 pc cm^{-3} curve is the rightmost. Sensitivities are scaled to 350 MHz using a spectral index of -1.6.

(A color version of this figure is available in the online journal.)

compared with higher-frequency surveys. However, 74% of our surveyed area is in directions with maximum expected DMs of less than 100 pc cm^{-3} for Galactic pulsars, as predicted by the NE2001 model.

Figure 3 shows the estimated sensitivity of the GBNCC survey compared with five past or ongoing surveys at DMs of 20, 50, 100, and 200 pc cm^{-3}. The GBNCC survey is about a factor of 2.5 more sensitive to low-DM pulsars in high Galactic latitude regions than the ongoing High Time Resolution Universe (HTRU; Keith et al. 2010) and High Time Resolution Universe North (HTRU-N; Barr et al. 2013) surveys being performed with Parkes and Effelsberg (Keith et al. 2010), is significantly more sensitive to MSPs than past Arecibo surveys, and has comparable sensitivity for MSPs to the ongoing Arecibo Drift 327 MHz survey (AO327; Deneva et al. 2013), which covers the declination range $0° > \delta > 38°$. We have not compared our sensitivity to Galactic plane surveys, such as the Pulsar Arecibo L-Band Feed Array (PALFA) survey (Cordes et al. 2006; Lazarus 2013), the Parkes Multibeam Pulsar Survey (PMPS; Manchester et al. 2001), and the HTRU mid- and low-latitude surveys (Keith et al. 2010) as these searches focus on low Galactic latitudes, where we are not as sensitive due to higher T_{sky}, dispersive smearing, and scattering—all of which are much larger effects in our frequency range.

To estimate the number of millisecond pulsars detectable by the GBNCC, we have carried out simulations using the snapshot population model described by Lorimer (2013), which is normalized to match the results of the PMPS (Manchester et al. 2001). Since this model provides pulsar luminosities at 1.4 GHz, we have assumed an underlying radio spectral index distribution with a mean of -1.4 and unit standard deviation, as found for the normal pulsar population by Bates et al. (2013) to scale the luminosities to 350 MHz. Under these assumptions, the total number of MSPs expected to be detectable in Stage I

of the survey is $\sim$30. The full survey is expected to detect of order 130 MSPs total. Future work will examine this population in more detail to constrain the spectral index and luminosity distributions of MSPs.

3. DATA ANALYSIS

For all-sky, high time/frequency resolution surveys such as the GBNCC, the data volume is very large. The entire survey will result in about 700 terabytes of raw data. In addition to a large data volume, the algorithms used to search the data require large amounts of computer time and typically require high performance computing (HPC) clusters. The majority of the data analysis for the GBNCC survey has been conducted using two HPC systems. The Guillimin cluster operated by CLUMEQ and Compute Canada has accounted for about 80% of processing to date, while the Lonestar and Ranger Clusters operated by the Texas Advanced Computing Center has accounted for the remaining 20%. We have recently begun processing data on a third HPC system at the University of Wisconsin-Milwaukee.

The data analysis process consists of RFI excision, correction for the effects of interstellar dispersion, a search for periodic signals, a single-pulse search, sifting of candidates, and then human inspection of diagnostic plots created by the search algorithms. The following subsections describe each of these pieces in more detail.

3.1. RFI Excision

The data are first analyzed using the `rfifind` tool from the PRESTO[20] (Ransom 2001) pulsar analysis package in order to find and mask RFI found in the data. The data are read in for each radio frequency channel in 2 s increments. For

---

each of the 2 s segments, the time domain mean and standard deviation are calculated, and a power spectrum is computed via Fourier transform and the highest Fourier power (with non-zero frequency) is recorded. For the time domain analysis, any segment for which the mean or standard deviation deviated by more than 10σ from that parameters median value over the entire observation is flagged to be masked during the remaining data analysis. Similarly, if a periodic signal was found in the power spectrum at a level of greater than 4σ, that segment was also marked to be masked. If more than 70% of channels are flagged in a single time interval, then all the channels are masked for that time interval. Similarly, if more than 30% of the time intervals are flagged in a single channel then all of that time intervals for that channel are flagged. For observations processed to date, the median masking fraction is 1.93% and less than 2% of the pointings have required masking fractions greater than 30%. In addition to the above RFI excision, known sources of RFI, such as the 60 Hz AC power line signal, are explicitly removed from the frequency domain after the de-dispersion step described in the following subsection and after the time series has been Fourier transformed.

3.2. Dispersion Removal

After initial RFI masking, the data are de-dispersed at 17,352 trial DMs ranging from 0 to 500 pc cm^{-3}. This set of DMs is created such that smearing due to an incorrect DM is less than the smearing within the frequency channels. Also, when the smearing time within the frequency channels is 2^N times the sample time, the time series is downsampled by a factor of 2^N. Due to the discovery of Fast Radio Bursts (Lorimer et al. 2007; Thornton et al. 2013), which are transients that may be of extra-galactic origin, we have recently increased our maximum DM. Beginning in 2014, we increased our DM range from 0 to 500 pc cm^{-3} to 0 to 3000 pc cm^{-3}, which now includes 26,532 trial DMs. We are searching all new data with this larger DM range and plan to re-process all of the already processed data with this new DM range. At 350 MHz, the dispersive smearing within a frequency channel for DMs of 500, 1000, and 3000 pc cm^{-3} is 2.4, 4.7, and 14.2 ms, respectively.

3.3. Periodic Search

Each of the de-dispersed time series is then Fourier trans-formed and the frequencies and harmonics associated with known sources of RFI are removed. The resulting time series are then searched for periodicities using the `accelsearch` tool from PRESTO. Two searches are performed, one allowing no acceleration search and one allowing signals to have a maxi-mum frequency bin drift of $\pm(50/n_{\mathrm{harm}})$ bins, where n_{harm} is the largest harmonic at which the signal was detected (Ransom et al. 2002). For the low-acceleration search, up to 16 harmonics are summed and for the high-acceleration search, up to 8 harmon-ics are summed (in powers-of-two harmonics). The candidates for each DM and for each of the two acceleration searches are stored for comparison after all DMs have been searched.

Once all DM trials have been searched, the periodicity candidates for the two acceleration searches are gathered into two separate lists. Within each list, candidates within ±1.1 Fourier bins of each other are combined into a single candidate and harmonically related candidates are removed. The resulting list of candidates is passed through a filter that removes candidates that only appeared at one DM. Then the candidate lists from the two acceleration searches are compared to one

another so that duplicate candidates can be removed (preference is given to the candidate with higher significance). Candidates whose power in the Fourier domain are greater than 6σ above the Gaussian noise level are folded, with up to 20 candidates being folded from the search with no acceleration and 10 candidates folded from the high acceleration searches. The candidates are Folded using the PRESTO tool `prepfold`, which creates diagnostic plots for human inspection. An example of the resulting diagnostic plot is shown in Figure 4.

3.4. Single-Pulse Search

Each of the de-dispersed time series is also searched for single pulses using a box car matched-filtering algorithm using the PRESTO tool `single_pulse_search.py`. The algorithm compares the data to boxcars with widths ranging from 81.92 μs to 100 ms. Pulses with S/Ns greater than 5 are stored. Though the lowest S/N RRAT confirmed so far has an S/N of 10, we save pulses down to S/Ns of 5 to establish the noise floor and to provide additional information useful for algorithms used to sift through potential single pulse candidates. Also, RRATs have been found in previous surveys with S/Ns of about 5, including some of the originally discovered RRATs (McLaughlin et al. 2006; M. A. McLaughlin 2014, private communication). After all de-dispersed time series have been searched, four plots are created for human inspection. Plots are created for the following DM ranges: 0–30, 20–110, 100–310, and 300–500 pc cm^{-3}. An example single-pulse plot is shown in Figure 5.

The single-pulse output is then processed through a sifting algorithm (C. Karako-Argaman et al. 2014, in preparation), which compares clusters of single-pulse events to the behavior expected of astrophysical sources. The algorithm then identifies the most promising candidates, thereby significantly reducing the number of plots to be visually inspected.

3.5. Candidate Inspection

A major obstacle for a large-scale pulsar survey such as the GBNCC is the inspection of the millions of candidates that are generated. To date, The GBNCC survey has generated over 1.2 million candidate plots. The GBNCC team has used a combination of computing algorithms and the help of high school and undergraduate students to analyze the large volume of candidates. Until recently, the data processed at each facility has been kept separate and analyzed individually. The candidates resulting from data processed by the Guillimin cluster have been inspected using a cursory examination based on signal strength. About 200,000 candidates have been generated from data processed on TACC resources and were entered into a web based candidate rating tool called ARCC Explorer (K. Stovall et al., in preparation). These candidates were pre-sorted using the PEACE algorithm (Lee et al. 2013) and all 200,000 candidates have been examined by at least one person with extensive experience looking at pulsar candidate plots or at least three students, who can have varying experience looking at such candidate plots. Though it is difficult to determine whether or not all pulsars in this set have been found, it is unlikely that an undiscovered pulsar with S/N above about 8 exists in the candidates. Beginning in late 2013, the results from each of the processing sites have begun to be combined into one complete set available to all members of the collaboration hosted by the CyberSKA infrastructure.[21] This combined data set is being
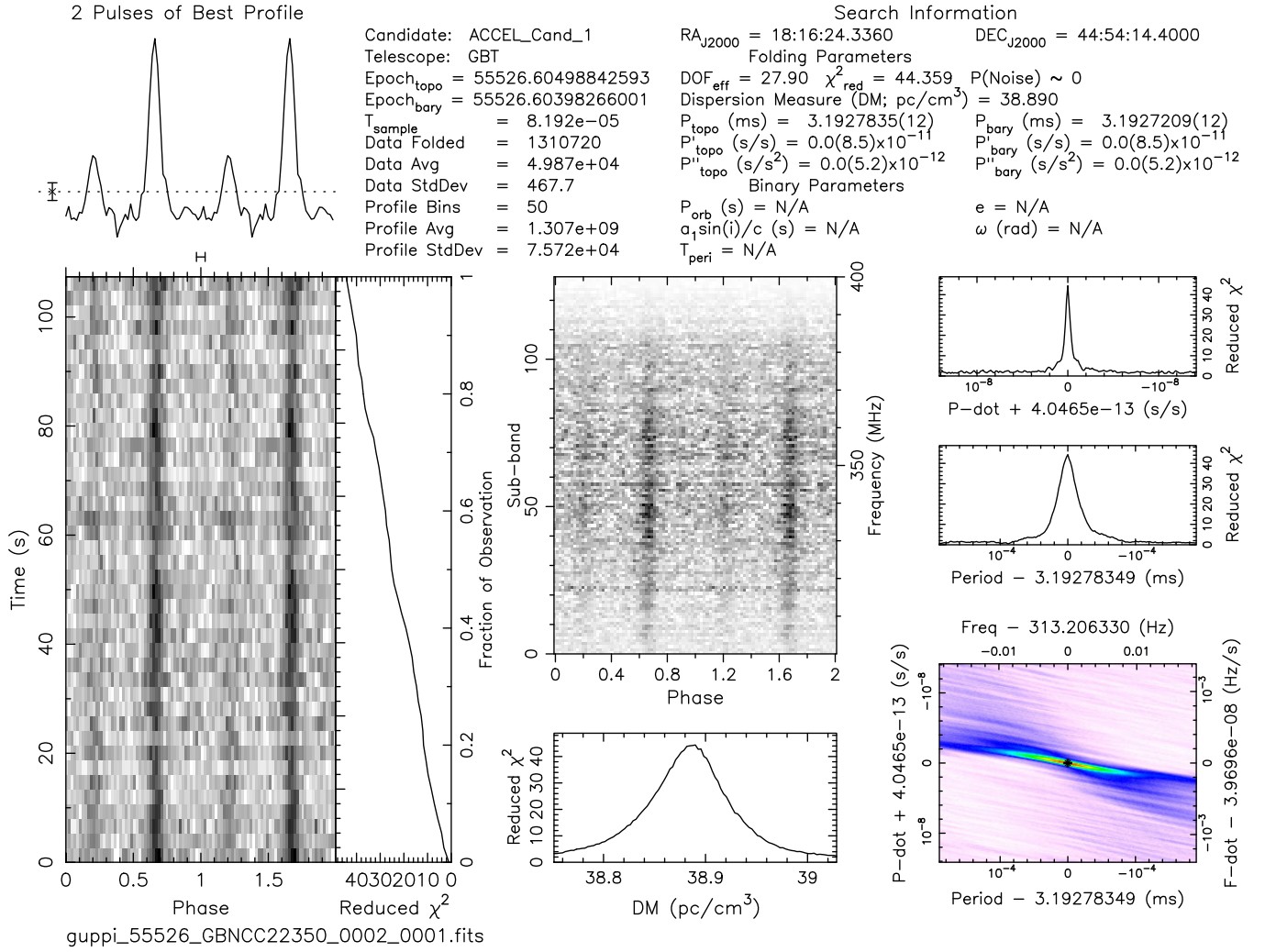
---

[21] http://www.cyberska.org/

Figure 4. Example periodic diagnostic plot from the GBNCC pipeline. This plot shows the GBNCC-discovered PSR J1816+4510.
(A color version of this figure is available in the online journal.)

thoroughly examined by eye and we are employing computer algorithms such as PEACE and image pattern recognition software described in Zhu et al. (2014) to pre-sort the candidates to find new pulsars as quickly as possible.

4. RE-DETECTIONS

About 80% of the data analysis for the section of sky north of $\delta = 38°$ has been completed. Inspection of the resulting candidates is ongoing, but to date, we have detected 75 of the known pulsars in this region of the sky. Table 5 in the Appendix contains a list of the re-detected sources, their distance from the center of the GBNCC beam (r), and the observed mean flux density at 350 MHz (S^o_{350}) of the detection. The ATNF database lists a total of 158 known pulsars in this region of the sky. However, this number contains many pulsars that are too weak to be detected in our survey as well as 15 sources that have not been detected at radio frequencies.

We evaluated whether or not our theoretically estimated sensitivity is comparable to our achieved sensitivity using the following method. First, we identified beams in which a known pulsar was within the $18'$ HWHM of the 350 MHz beam as taken from The Proposer's Guide for the Green Bank Telescope.[22]

Then we identified which of these sources had a mean flux density reported in the ATNF database at either 400 MHz (S_{400}) or 1400 MHz (S_{1400}). For each source with one of these mean flux densities reported, we extracted S_{400} and S_{1400}. We then estimated a theoretical mean flux density at 350 MHz (S^t_{350}) by calculating the spectral index for the source from S_{400} and S_{1400}, if both values were available. We used this spectral index to estimate S^t_{350}. In cases with only one mean flux density value available in the ATNF database, we used a spectral index of -1.7 to scale the reported value to 350 MHz. There can be large uncertainties in the measurements for S_{400} and S_{1400} in the ATNF database, so our resulting S^t_{350} is a very rough estimate of the theoretical mean flux density at 350 MHz. We then took the observed S/N (S/N_o) and used Equation (1) to get an observed mean flux density (S^o_{350}) for each source using the parameters of our survey and W_{50} for the source as reported by the ATNF database. For cases without a reported W_{50}, we fit a set of Gaussians to the profile from our detection and used the FWHM from these Gaussians as W_{50}. We also adjusted the value for T_{sys} for each sky location by taking the value for T_{sky} at 408 MHz reported in Haslam et al. (1982) and scaling to 350 MHz using the spectral index -2.6.

Comparison of S^t_{350} to S^o_{350} revealed that 37% of the 59 detections satisfying our requirements were detected with a S^o_{350}
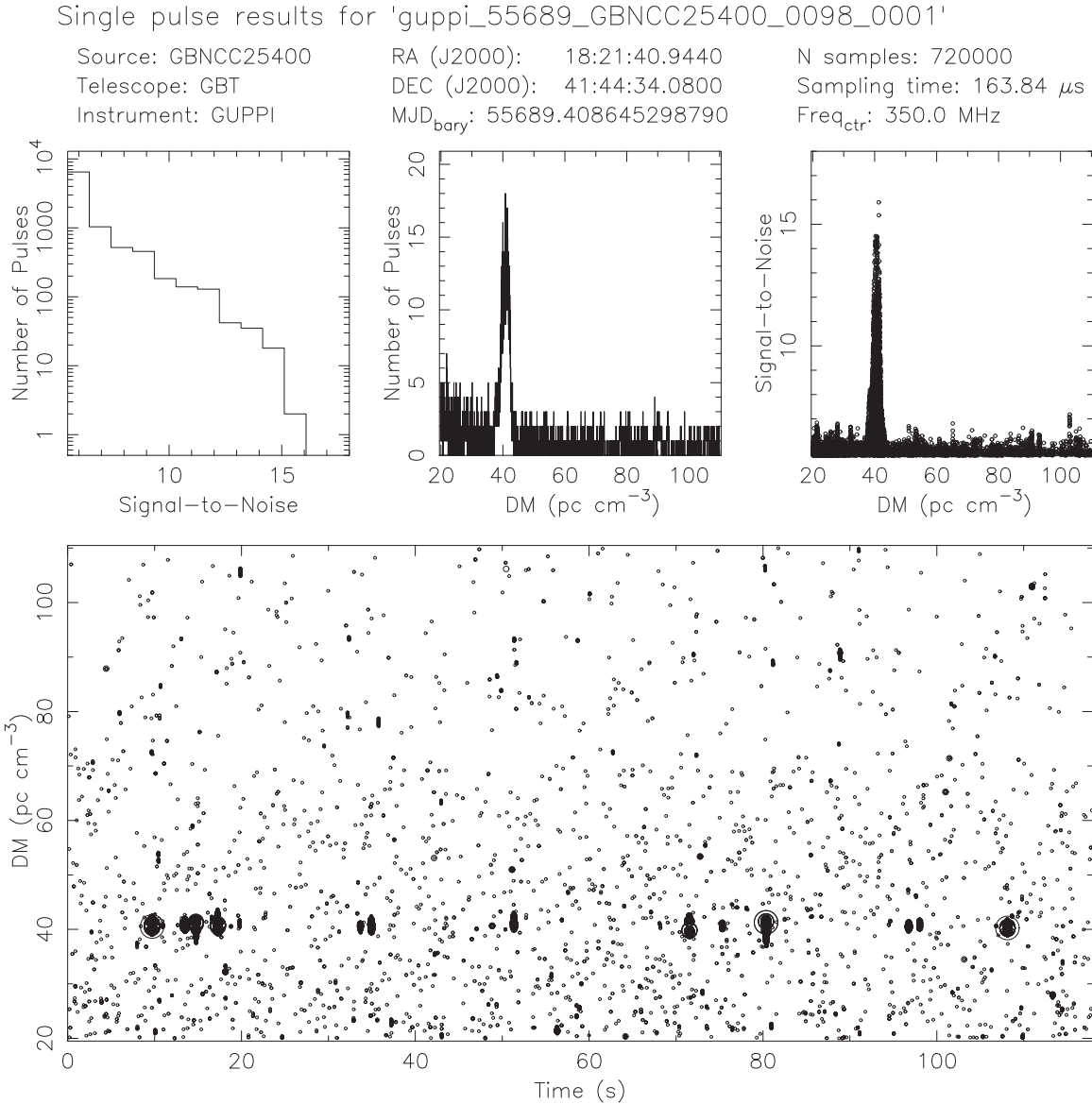
Figure 5. Single-pulse plot from the GBNCC pipeline. The signal resulting from pulses of astrophysical origin can be seen at a DM of 40 pc cm^{-3} as this particular beam contains the GBNCC-discovered PSR J1821+41. Typical detections of RRATs look similar, but generally have fewer detected pulses than shown here and in some cases only a single pulse may be detected. The change in the density of points at around 70 pc cm^{-3} is due to the down-sampling factor changing by a factor of two.

larger than expected, another 22% were within a factor of two of S_{350}^t, and a total of 78% were within a factor of four. Figure 6 shows a scatter plot of S_{350}^t and S_{350}^o. In addition to the rough estimate of the spectral properties for each pulsar, there are many additional factors that can affect individual observations including but not limited to interstellar scintillation, pulsar nulling, and RFI. Another factor, in the case of slow pulsars, is that our integration time of 120 s does not allow for a large number of pulses, so normal pulse-to-pulse variability can affect the observed S/N. Of the 59 detections, there were six observations for which the ratio of S_{350}^t/S_{350}^o was 8 or larger. Visual inspection of these six detections revealed that three of them showed evidence of nulling and the other three had intensities that were variable throughout the observation. Also, three of them were near the 18′ HWHM of the 350 MHz receiver and one was severely affected by RFI. We conclude that our expected to true sensitivity are roughly in agreement, given all of the assumptions involved.

5. PULSAR TIMING ANALYSIS

In Section 6, we present timing solutions for five new GBNCC discoveries. Observations were conducted using a combination of GBNCC survey time at 350 MHz, dedicated follow-up projects (GBT11B-070 and GBT13A-458) at 820 MHz, and observations from a few smaller projects and in one case from NANOGrav observations. The observations taken during GBNCC survey time were typically 10 to 15 minutes in duration and use the same GBNCC observing setup described in Section 2. The 820 MHz observations of PSR J1816+4510 under project GBT11B-070 were typically 15 to 30 minutes in duration, while the observations of the pulsars in GBT13A-458 were typically four to five minutes in duration. The observations under GBT11B-070 and GBT13A-458 at 820 MHz had a bandwidth of 200 MHz divided into 2048 frequency channels and a sample time of 40.96 μs. Additional times of arrival (TOAs) for PSR J0645+5158 were obtained from the
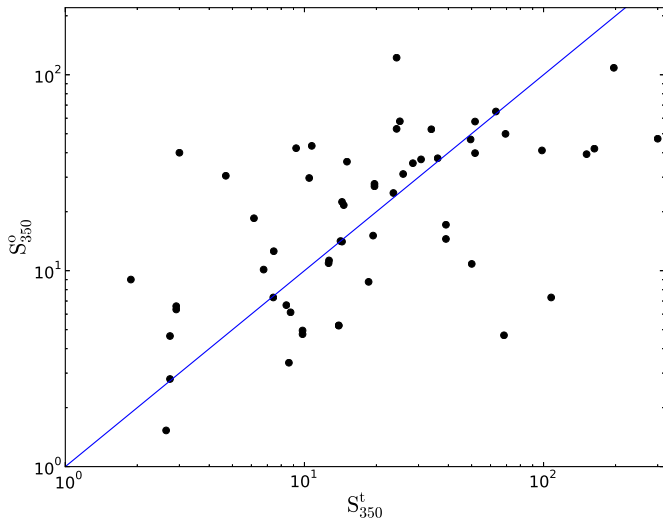
Figure 6. Theoretical mean flux density at 350 MHz (S_{350}^t) vs. the observed mean flux density at 350 MHz (S_{350}^o) for 59 detections of known pulsars with a measured mean flux density at either 1400 MHz or 400 MHz reported in the ATNF catalog and that are within 18′ of the center of a GBNCC pointing. The blue line represents where $S_{350}^t = S_{350}^o$.

(A color version of this figure is available in the online journal.)

NANOGrav collaboration due to it being a promising new candidate for inclusion in PTAs. The NANOGrav data consist of two sets of data, one at a center frequency of 820 MHz with 200 MHz of bandwidth divided into 128 coherently de-dispersed frequency bins, and one at a center frequency of 1500 MHz with 800 MHz of bandwidth divided into 512 coherently de-dispersed frequency bins. Both data sets were taken in fold mode with 2048 bins across the pulse profile and profiles were written out every 15 s. Two complete orbits (one at 1500 MHz and the other at 820 MHz) of PSR J1816 + 4510 were observed under the Fermi project GLST051395. This data was taken in the same mode as the NANOGrav data set described above. We also observed PSR J0645 + 5158 under the project GBT11A-075 and PSR J0636 + 5129 under project GBT12A-473 to reduce the positional uncertainty of each source. These observations consisted of 820 MHz, 1500 MHz, and 2200 MHz observations. The 820 MHz observations were taken in the same mode as our main timing observations, while the higher frequency observations were each taken with 800 MHz of bandwidth across 2048 frequency channels with a sample time of 40.96 μs.

For each of the pulsars, we created template profiles by first summing together multiple observations and then fitting the resulting high signal-to-noise ratio profiles to Gaussians using a least-squares minimization algorithm.[23] For each pulsar, the number of Gaussian components needed to represent the profile did not change from one frequency to another, however the FWHM did change, so we used the 820 MHz profile, but modified the FWHM for other frequencies. Using the template profile, we calculated TOAs of pulses using a least-squares fit in the Fourier domain (Taylor 1992).[24] In the case of the isolated pulsars and the long-period binary pulsar J0214 + 5222, we divided the observations into two frequency bands and obtained two TOAs from each band for a total of four TOAs per observation. For the short-period binary pulsars, we initially summed the frequency channels into a single sub-band and obtained five TOAs from each observation in order to sample

more of the pulsar's orbital phase. Once we solved these pulsars' orbits, we then divided the observation into two frequency sub-bands and obtained two TOAs from each sub-band. We used these TOAs to obtain a timing solution by accounting for every rotation of the pulsar using the TEMPO[25] software package.

Each of our timing solutions use the DE421 Solar System ephemeris and TT(BIPM) clock corrections. For each pulsar, we obtained good timing solutions with no systematic trends. For four of the five pulsars, we multiplied each TOA uncertainty by an error factor (values range from 1.0 to 1.5) in order to get a reduced χ^2 near one. This ensures that the fitted parameters and their errors are justified by the actual TOA rms. We did not do this for PSR J0214 + 5222 because several parameters are still highly covariant due to sparse coverage of the orbit, so its χ^2 is less than one.

6. DISCOVERIES

Prior to the ongoing full data analysis, we performed a preliminary search of the GBNCC data by selecting beams containing a gamma-ray point source as identified by *Fermi*. This method led to the search of 128 of the ≈30,000 beams from stage 1 of the GBNCC survey. This search resulted in the detection of what appeared to be two new MSPs. Comparison with recent *Fermi* Pulsar Search Consortium discoveries revealed that one of them (J2302 + 4442) had been previously discovered (Cognard et al. 2011), but the other (J1816 + 4510) was a previously unknown MSP. PSR J1816 + 4510 is described in detail below.

After this preliminary data analysis was complete, we began processing the data in earnest, which as of 2014 March 18 has resulted in the discovery of 67 pulsars, including 9 MSPs and 6 intermediate-spin-period pulsars. Additionally, seven RRATs have been discovered that will be presented in C. Karako-Argaman et al. (2014, in preparation). Figure 2 shows our discovered sources on the sky. We highlight that we are finding MSPs spread across the sky, which is essential for the efforts of the PTAs to detect the stochastic background from GW sources.

Discovery parameters for 62 discovered pulsars are given in Table 1. The parameters included are the observed spin period, DM, position, an estimated distance using the DM, the discovery S/N (S/N_{Disc}), and an estimated mean flux density at 350 MHz (S_{350}^o). The mean flux density was estimated by putting the parameters for the GBNCC survey, the discovery S/N, and the FWHM from the discovery pulse profile into Equation (1). We present timing solutions for five of the pulsars in Tables 2–4 and show their pulse profiles at 149, 350 MHz, 820 MHz, and 1500 MHz (where applicable) in Figure 7. The profiles at 350 MHz, 820 MHz, and 1500 MHz were made using data described in Section 5, while the 149 MHz profiles are from LOFAR. The LOFAR profiles are averages over 10–60 minutes, using 78 MHz of bandwidth centered at 149 MHz. The data were coherently de-dispersed within each of 400 195-kHz frequency subbands (see Stappers et al. 2011 for further details of this observing mode). Figure 8 shows timing residuals for the five pulsars for which we are presenting timing solutions. Follow-up observations and analysis of the 62 pulsars for which we did not present timing solutions as well as the 7 RRATs are ongoing and timing solutions will appear in future publications.

Two of the pulsars (J0645 + 5158 and J1434 + 7257) are isolated and their timing solutions are presented in Table 2. The other three pulsars (J0214 + 5222, J0636 + 5129, and J1816 + 4510) are binary pulsars. In the case of J0636 + 5129

---

[23] PRESTO's `pygaussfit.py`
[24] PRESTO's `get_TOAs.py`, which uses the FFTFIT routine

[25] http://tempo.sourceforge.net

Table 1
Discovery Parameters for 62 GBNCC Discovered Pulsars

Pulsar	P (s)	DM (pc cm^{-3})	R.A. (hh:mm)	Decl. (dd:mm)	D[a] (kpc)	S/N$_{\rm Disc}$	S$^{\rm o}_{350}$ (mJy)
J0034 + 69	0.03680412(16)	80.0(3)	00:34(3)	69:43(18)	2.8	61.2	4.5
J0053 + 69	0.832938(28)	117(2)	00:53(3)	69:39(18)	4.3	676.9	30.5
J0059 + 50	0.996009(61)	67(2)	00:59(2)	50:02(18)	2.7	120.0	5.6
J0112 + 66	4.30124(70)	112(3)	01:12(3)	66:22(18)	3.4	340.1	13.6
J0125 + 62	1.708233(98)	118(2)	01:26(3)	62:35(18)	3.9	50.9	3.4
J0136 + 63	0.717895(27)	286(2)	01:36(3)	63:42(18)	>44.3[b]	40.3	3.3
J0141 + 63	0.04668588(49)	272.6(4)	01:41(2)	63:08(8)	>44.3[b]	13.1	1.3
J0213 + 52	0.376384(15)	38(2)	02:13(2)	52:32(8)	1.5	67.6	4.1
J0325 + 67	1.364741(62)	65(2)	03:26(3)	67:49(18)	2.3	816.4	26.3
J0338 + 66	1.76200(15)	67(2)	03:39(3)	66:44(18)	2.2	260.2	10.5
J0358 + 42	0.2264777(50)	46(1)	03:58(1)	42:06(9)	1.6	84.0	5.5
J0358 + 66	0.09150682(63)	62.3(4)	03:58(3)	66:40(18)	2.2	103.8	5.3
J0417 + 61	0.440283(13)	71(2)	04:17(3)	61:08(18)	2.3	31.4	1.5
J0510 + 38	0.07656440(44)	69(1)	05:09:59(40)	38:12(8)	1.9	33.1	3.4
J0519 + 54	0.340194(12)	43(1)	05:20(2)	54:25(18)	1.5	63.7	3.8
J0610 + 37	0.443861(14)	39(2)	06:11(2)	37:18(18)	1.2	29.0	1.3
J0614 + 83	1.039203(51)	44(1)	06:14(10)	83:14(18)	2.2	57.8	1.9
J0645 + 80	0.657873(24)	50(3)	06:46(7)	80:09(18)	2.8	119.0	5.5
J0737 + 69	6.82424(63)	16(3)	07:37(2)	69:14(8)	0.73	59.4	1.2
J0740 + 41	0.0031392150(48)	20.83(9)	07:41(1)	41:04(8)	0.71	47.6	5.8
J0741 + 66	0.00288570374(45)	14.96(4)	07:42(2)	66:20(8)	0.67	365.1	32.5
J0746 + 66	0.4076702(93)	28(1)	07:46(3)	66:36(18)	1.4	273.3	7.4
J0750 + 57	1.174875(65)	27(2)	07:50(2)	57:00(18)	1.0	55.8	2.9
J0943 + 41	2.229489(99)	21(2)	09:43(2)	41:09(18)	0.79	550.1	8.6
J1101 + 65	3.63132(53)	19(3)	11:02(3)	65:07(18)	0.82	509.2	10.4
J1110 + 58	0.793348(21)	26(1)	11:11(3)	58:52(18)	1.3	65.9	1.6
J1122 + 78	0.0042013838(14)	11.22(8)	11:25:58(9)	78:23(2)	0.62	274.5	17.1
J1320 + 67	1.028620(35)	28(2)	13:20(3)	67:30(18)	1.5	33.7	1.4
J1627 + 86	0.3957850(87)	46(1)	16:27(5)	86:54(4)	3.0	199.9	5.6
J1629 + 43	0.1811729(16)	7.3(8)	16:29(2)	43:59(18)	0.61	99.4	3.2
J1647 + 66	1.599819(50)	23(2)	16:48(1)	66:04(8)	1.2	147.1	3.3
J1649 + 80	0.0020210978(13)	31.09(4)	16:50(4)	80:45(8)	1.6	69.7	4.1
J1706 + 59	1.476687(58)	31(2)	17:07(3)	59:10(18)	1.8	369.6	8.0
J1710 + 49	0.0032202231(21)	7.09(8)	17:10:29(13)	49:20(2)	0.66	117.4	14.1
J1800 + 50	0.578364(15)	23(2)	18:01(2)	50:28(18)	1.4	702.6	23.5
J1815 + 55	0.426802(13)	59(2)	18:15(2)	55:29(18)	>50.0[b]	108.2	4.2
J1821 + 41	1.261787(46)	40(3)	18:22(3)	41:45(18)	2.5	115.5	2.6
J1859 + 76	1.393617(87)	47(2)	18:59(6)	76:54(18)	2.9	106.3	3.3
J1911 + 37	0.851095(33)	72(2)	19:11(2)	37:38(18)	4.2	216.6	7.0
J1921 + 42	0.595201(15)	53(1)	19:21:56(40)	42:25(8)	3.2	180.9	8.1
J1922 + 58	0.529623(10)	53(1)	19:22(3)	58:28(18)	3.3	79.0	3.1
J1929 + 62	1.456004(66)	67.7(7)	19:29(3)	62:16(18)	6.4	38.1	1.4
J1935 + 52	0.568387(17)	71(2)	19:35(2)	52:12(18)	4.4	52.3	3.1
J1939 + 66	0.022260606(52)	41.2(1)	19:40(3)	66:12(18)	2.3	46.4	2.1
J1941 + 43	0.840887(35)	79(2)	19:42(2)	43:23(18)	4.3	213.6	9.1
J1942 + 81	0.2035682(44)	40.3(5)	19:42(3)	81:06(8)	2.1	175.9	4.8
J1953 + 67	0.008565431(18)	57.2(1)	19:53(3)	67:02(18)	3.4	29.5	1.7
J1954 + 43	1.386961(94)	130(3)	19:55(2)	43:50(18)	6.9	22.5	2.8
J2001 + 42	0.719161(22)	55(1)	20:02(3)	42:43(18)	3.3	321.0	20.2
J2017 + 59	0.403619(12)	61(3)	20:18(3)	59:13(18)	3.2	10.5	1.1
J2027 + 74	0.515229(14)	11(3)	20:28(5)	74:47(18)	0.9	30.7	2.4
J2105 + 28	0.405737(11)	62.4(8)	21:06(2)	28:29(18)	3.7	249.8	8.6
J2113 + 67	0.5521697(88)	55.1(8)	21:14(3)	67:02(18)	2.7	26.6	1.0
J2122 + 54	0.1388657(13)	31.7(7)	21:23(1)	54:33(8)	2.1	40.1	3.4
J2137 + 64	1.75087(14)	106(2)	21:37(3)	64:19(18)	4.6	167.2	6.4
J2205 + 62	0.3227871(63)	167(3)	22:06(3)	62:04(18)	6.7	8.6	1.2
J2207 + 40	0.6369852(85)	12(2)	22:07(2)	40:57(18)	1.0	59.5	3.8
J2210 + 57	2.05743(13)	189.43(6)	22:11(3)	57:29(18)	6.1	9.9	1.1
J2229 + 64	1.89312(13)	194(1)	22:29(3)	64:58(18)	>46.9[b]	56.1	3.4
J2243 + 69	0.855405(32)	68(2)	22:44(7)	69:40(18)	2.9	78.8	3.2
J2316 + 69	0.813386(22)	71(2)	23:17(3)	69:12(18)	2.8	51.9	2.5
J2353 + 85	1.011691(37)	38(2)	23:54(7)	85:34(8)	1.9	183.6	4.9

Notes.

[a] Distances are from the NE2001 electron model with ~20% uncertainty in distance values (Cordes & Lazio 2002).

[b] DM values are slightly larger than the expected highest DM given by the NE2001 electron model and therefore the model does not give reliable distances for these sources. The maximum DM values expected along these lines of sight are 212, 205, 51, and 187 pc cm^{-3} for PSRs J0136 + 63, J0141 + 63, J1815 + 55, and J2229 + 64, respectively.

Table 2
Timing Solutions and Derived Parameters for the Isolated PSRs J0645 + 5158 and J1434 + 7257

Parameter	PSR J0645+5158	PSR J1434+7257
Timing Parameters		
Right ascension (J2000)	06:45:59.08191(1)	14:33:59.7370(9)
Proper motion in R.A. (mas yr^{-1})	1.2(1)	$\cdots$
Declination (J2000)	51:58:14.9210(1)	72:57:26.512(6)
Proper motion in Decl. (mas yr^{-1})	$-7.5(2)$	$\cdots$
Parallax (mas)	1.4(4)	$\cdots$
Pulsar period (s)	0.00885349668613151(7)	0.04174114783993(3)
Period derivative (s s^{-1})	$4.923(8) \times 10^{-21}$	$5.50(1) \times 10^{-19}$
Dispersion measure (pc cm^{-3})	18.247536(9)	12.605(1)
Reference epoch (MJD)	56143.0	55891.0
Span of timing data (MJD)	55700–56586	55196–56585
Number of TOAs	3747	127
RMS residual (μs)	0.51	58
350 MHz Flux (mJy)	2.4	1.3
820 MHz Flux (mJy)	0.37	0.34
FWHM 350 MHz (ms)	0.23	1.6
FWHM 820 MHz (ms)	0.086	1.9
Derived Parameters		
Galactic longitude	163.96	113.08
Galactic latitude	20.25	42.15
Lutz-Kelker adjusted parallax (mas)	1.0(4)	$\cdots$
DM-derived distance (kpc)	0.7	0.7
PX-derived distance (kpc)	$0.7^{+0.2}_{-0.1}$	$\cdots$
Shklovskii Adjusted period derivative (s s^{-1})	$4.1^{+0.2}_{-0.3} \times 10^{-21}$	$\cdots$
Surface magnetic field strength (10^8 G)	1.9	48
Spindown Luminosity (10^{32} erg s^{-1})	2.4	3.0
Characteristic age (Gyr)	34	1.2

Notes. Numbers in parentheses represent 1σ uncertainties in the last digits as determined by TEMPO, scaled such that the reduced $\chi^2 = 1$. All timing solutions use the DE421 Solar System Ephemeris and the UTC(BIPM) time system. Derived quantities assume an $R = 10$ km neutron star with $I = 10^{45}$ gm cm^2. The DM derived distances were calculated using the NE2001 model of Galactic free electron density, and have typical errors of $\approx 20\%$ (Cordes & Lazio 2002). The parallax and parallax distance was determined using TEMPO and then corrected for Lutz-Kelker bias using the technique described in Verbiest et al. (2010). The Shklovskii adjusted period derivative is corrected for the Shklovskii effect (Shklovskii 1970) using the proper motion and PX-derived distance. The surface magnetic field strength, spindown luminosity, and characteristic age were calculated using the Shlovskii adjusted period derivative.

and J1816 + 4510, the orbits are short-period and highly circular, so we have used the ELL1 tempo model (see Appendix of Lange et al. 2001). PSR J0214 + 5222 is in a very long-period orbit, which is more eccentric and therefore we have used the BT tempo model (Blandford & Teukolsky 1976). The solution for the long-period binary, J0214 + 5222, is given in Table 3 and the solutions for the short-period binaries are given in Table 4. Figure 1, described in Section 1, shows the minimum mass and orbital periods of our short-period binary discoveries plotted among previously known binary pulsars with spin periods below 10 ms. This plot shows how our discovered binaries (blue stars) compare to the known populations of MSPs with white dwarf companions (unfilled, black circles) as well as redback (red circles), black widow systems (black circles), and the "diamond planet" systems (black diamonds). Additional details about our discovered systems are given in the subsections below.

6.1. PSR J0214 + 5222

PSR J0214 + 5222 (hereafter "J0214") is an intermediate-period pulsar with a spin period of 24.5 ms and a DM of 22 pc cm^{-3}. This pulsar is in a long-period, nearly circular orbit of about 512 days with a projected semi-major axis of 175 lt-s. The minimum (where inclination = 90°) and median (assuming

a distribution of random inclinations) companion masses are 0.42 $M_\odot$ and 0.49 $M_\odot$, respectively. We compared the position to archival optical catalogs and found a possible counterpart at the position of J0214 in Second Generation Digitized Sky Survey (DSS-2) images. In December of 2012, we observed the field containing J0214 with the S2KB imager[26] on the 0.9 m WIYN[27] telescope. We took 6 × 10 minutes dithered exposures in the B (2012 December 11) and R (2012 December 12) filters. The data were reduced using normal procedures in IRAF: we subtracted the bias using an overscan region and separate bias frames, corrected the images using flatfields, and combined the individual exposures. Astrometric solutions were derived relative to the UCAC3 catalog (Zacharias et al. 2009): we fit for plate-scale, rotation, and center using 350 stars and found a solution with an rms of 0″.1 in each coordinate. We determined a photometric solution for each night using observations of the Stetson (2000) standard field L98. About 750 stars were used for the solution (which we corrected to the airmass of the J0214 observations using the Kitt Peak extinction curves[28]), and we

---

[26] http://www.noao.edu/0.9m/observe/s2kb.html
[27] http://www.noao.edu/0.9m/
[28] See http://www.noao.edu/kpno/manuals/dim/#trans.

Table 3
Timing Solution and Derived Parameters for the Long-period
GBNCC Discovered Pulsar J0214 + 5222

Parameter	PSR J0214+5222
Timing Parameters	
Right ascension (J2000)	02:14:55.2713(34)
Declination (J2000)	52:22:40.95(19)
Pulsar period (s)	0.02457529479071(22)
Period serivative (s s^{-1})	2.99(10) $\times 10^{-19}$
Dispersion measure (pc cm^{-3})	22.0354(34)
Reference epoch (MJD)	55974.0
Span of timing data (MJD)	55353–56594
Number of TOAs	69
RMS residual (μs)	75
350 MHz Flux (mJy)	0.90
820 MHz Flux (mJy)	0.24
FWHM 350 MHz (ms)	1.2
FWHM 820 MHz (ms)	2.5
Binary Parameters	
Orbital period (days)	512.0397(3)
Projected semi-major axis (lt-s)	174.5658(2)
Epoch of periastron (MJD)	56126.61(1)
Orbital eccentricity	0.0053283(5)
Longitude of periastron (deg)	210.59(1)
Mass function ($M_\odot$)	0.02178
Minimum companion mass ($M_\odot$)	0.4157
Derived Parameters	
Galactic longitude	135.63
Galactic latitude	−8.42
DM-derived distance (kpc)	1.0
Surface magnetic field strength (10^8 G)	27
Spindown luminosity (10^{32} erg s^{-1})	8.0
Characteristic age (Gyr)	1.3

Notes. The notes for Table 2 also apply to this table. Minimum companion masses were calculated assuming a 1.4 $M_\odot$ pulsar.

estimate zero-point uncertainties of about 0.05 mag. The images are shown in Figure 9.

We see an object extremely close to the position of the pulsar. This source is within 0″.16 of the radio timing position, which we compare with an estimated astrometric uncertainty of 0″.2. We performed photometry using sextractor (Bertin & Arnouts 1996) and find $B = 21.48 \pm 0.06$ and $R = 21.72 \pm 0.09$ (including zero-point uncertainties). We estimate that there are 1.1×10^{-3} sources arcsec^{-2} with $B < 21.6$, so the chance of a false association is roughly 10^{-4}. Because of this, we consider it likely that we have detected the optical counterpart of the J0214 system, although we require spectroscopic confirmation to be certain.

It is already apparent from Figure 9 that the counterpart is rather blue. Most of the stars in the field have $B − R \approx 1$, while the counterpart has $B − R = -0.13 \pm 0.11$. However, with only two bands we cannot uniquely determine the effective temperature of the counterpart. Instead we estimate the extinction to be $A_V \approx 0.4$ mag at a distance of 1 kpc (the DM distance) using Drimmel et al. (2003). With that we infer an effective temperature of about 26,000 K and a normalization of $0.009\ R_\odot$ kpc^{-1}.

This result is curious. If the companion were a normal white dwarf, the high temperature implies a young age, varying between 18 Myr for the lowest possible masses to 110 Myr for 1 $M_\odot$ (we use the synthetic photometry and evolutionary models from Tremblay et al. 2011 and Bergeron et al. 2011 for

H and He atmospheres, respectively[29]). We have ignored any possible heating of the companion by the pulsar, but due to the long-period orbit this assumption seems reasonable. This age is much smaller than the characteristic age of J0214 (1.3 Gyr), and the radio discovery of such a system during the short-lived time that the white dwarf has such a high effective temperature seems rather fortuitous (also see Kaplan et al. 2014).

If the DM distance is close to correct, then the normalization is inconsistent with a companion mass near the minimum. Instead it would require a companion mass of about 0.9 $M_\odot$, implying that the inclination angle is ≈33° (although such a massive companion does relax the age constraint since the effective temperature would be less than the one inferred above). Instead, we might expect J0214 to be like other wide binaries with companions near 0.4 $M_\odot$, and an evolutionary path like that of helium-core white dwarfs (Tauris et al. 2012). The companion to J0214 is directly on the Tauris & Savonije (1999) curve if its mass is near the minimum value (inclination near edge-on). In that case, the distance would be closer to 2 kpc: not an unreasonable disagreement for a source at high Galactic latitude. However, we note that given the pulsar's spin period of 24.5 ms and period derivative of 3×10^{-19} the pulsar is not fully recycled, so the validity of the Tauris et al. (2012) scenario is not clear.

A possible resolution to the age question that makes the distance disagreement even worse would be if the companion were a subdwarf B (sdB) star (Heber 2009). These objects, which can be slightly more massive than the most massive helium-core white dwarfs (around 0.45 $M_\odot$), more naturally have effective temperatures above 20,000 K due to core helium burning. Except for the mass, the evolution could be reasonably similar to that which produces a helium-core WD. However, sdB stars have radii of $\gtrsim$0.1 $M_\odot$, which would require a distance of >5 kpc. Reconciling this with the DM distance may be difficult, but as directed searches for pulsars around sdB start have so far not been successful (Coenen et al. 2011), it would make J0214 the first known PSR–sdB system. An optical spectrum should be able to distinguish between these scenarios given the very different surface gravities (10^7 cm s^{-2} for a 0.4 $M_\odot$ WD, up to 10^9 cm s^{-2} for a massive WD, and <10^6 cm s^{-2} for a sdB star).

6.2. PSR J0636 + 5129

Follow-up observations of PSR J0636 + 5129 (hereafter J0636) revealed that this bright, nearby MSP is in a binary system with a very short orbital period of 96 minutes (PSR J1311−3430 is the only rotation-powered pulsar in the Galactic Field with a shorter orbital period, by 2 minutes) and the pulsar's projected semi-major axis is 0.009 lt-s. Assuming a 1.4 $M_\odot$ pulsar mass, this implies that the minimum and median companion masses are about 7.4 M_J and 8.5 M_J, respectively. The DM of this system (11.1 pc cm^{-3}) indicates a distance of only 0.5 kpc, using the NE2001 model. Our timing up to this point has enabled a measurement of a proper motion of $5.2^{+1.3}_{-1.2}$ mas yr^{-1} and an annual parallax measurement of 4.7(5) mas. We corrected the parallax measurement for Lutz-Kelker bias as described by Verbiest et al. (2010) and get a value of 4.27(56) mas. The parallax measurement implies a distance of $0.21^{+0.03}_{-0.02}$ kpc. Combining our proper motion measurement with our parallax distance of 0.21 kpc implies a transverse velocity of 5 km s^{-1}. Even after accounting for the peculiar velocity of the sun, it is clear that J0636 did not receive a significant kick at birth and is among

---

[29] Also see http://www.astro.umontreal.ca/~bergeron/CoolingModels/.

Table 4
Timing Solutions and Derived Parameters for the GBNCC Discovered Binary PSRs J0636+5129 and J1816+4510

Parameter	PSR J0636+5129	PSR J1816+4510
Timing Parameters		
Right ascension (J2000)	06:36:04.84645(2)	18:16:35.93436(7)
Proper motion in R.A. (mas yr^{-1})	4.3(9)	5.3(8)
Declination (J2000)	51:28:59.9625(6)	45:10:33.8618(8)
Proper motion in Decl. (mas yr^{-1})	2(1)	$-3(1)$
Parallax (mas)	4.9(6)	$\cdots$
Pulsar period (s)	0.0028689528463143(1)	0.0031931035538505(2)
Period derivative (s s^{-1})	$3.38(3) \times 10^{-21}$	$4.310(1) \times 10^{-20}$
Dispersion measure (pc cm^{-3})	11.10598(6)	38.8874(4)
Reference epoch (MJD)	56307.0	56047.0
Span of timing data (MJD)	56028–56586	55508–56586
Number of TOAs	1180	457
RMS residual (μs)	2.6	8.7
350 MHz Flux (mJy)	1.8	1.5
820 MHz Flux (mJy)	0.66	0.28
FWHM 350 MHz (ms)	0.16	0.29
FWHM 820 MHz (ms)	0.15	0.24
Binary Parameters		
Orbital period (days)	0.0665513390(1)	0.3608934817(2)
Projected semi-major axis (lt-s)	0.0089859(1)	0.595405(1)
Epoch of ascending node (MJD)	56307.4294776(5)	56047.5490643(2)
Eccentricity sin(Omega)	$-1(3) \times 10^{-5}$	$5(3) \times 10^{-6}$
Eccentricity cos(Omega)	$-2(3) \times 10^{-5}$	$6(4) \times 10^{-6}$
Mass function ($M_\odot$)	1.759×10^{-7}	0.00174
Minimum companion mass ($M_\odot$)	0.007035	0.1619
Derived Parameters		
Galactic longitude	163.91	72.83
Galactic latitude	18.64	24.74
Lutz-Kelker adjusted parallax (mas)	$4.51^{+0.57}_{-0.58}$	$\cdots$
DM-derived distance (kpc)	0.5	2.4
PX-derived distance (kpc)	$0.203^{+0.027}_{-0.021}$	$\cdots$
Shklovskii adjusted period derivative (s s^{-1})	$3.373^{+0.044}_{-0.057} \times 10^{-21}$	$4.180^{+0.077}_{-0.121} \times 10^{-20}$
Surface magnetic field strength (10^8 Gauss)	1.0	4.0
Spindown luminosity (10^{32} erg s^{-1})	56	510
Characteristic age (Gyr)	14	1.2

Notes. The notes for Tables 2 and 3 also apply to this table. The Shklovskii adjusted period derivative for PSR J1816+4510 was calculated using the distance from Kaplan et al. (2013) since we do not have a measurable parallax.

the lowest of all currently published values. From the Galactic latitude for J0636 (18°.6) and the parallax distance mentioned above, we calculate a distance from the Galactic plane (z-height) for this pulsar of only 0.06 kpc, which is consistent with its low transverse velocity.

Initial assessment of this system based on the orbital period and companion mass would suggest that this system is potentially related to the black widow class of pulsars. In fact, the orbital period and companion mass of J0636 are very similar to the recently discovered black widow system J1311−3430 (Pletsch et al. 2012; Romani et al. 2012; Ray et al. 2013). However, unlike J1311−3430 and most other black widow systems, J0636 does not exhibit eclipses and there are no signs of delays due to DM variations caused by excess material in the system (see Figure 10). Nor are there any signs of changes in the orbital period over time. The fact that these effects, which are commonly seen in black widow systems, are absent may indicate that the system is instead related to the "diamond planet" system (J1719−1438; Bailes et al. 2011), which consists of an MSP in a 140 minute orbit with a 1.2-M_J companion. We note that there are some black widow systems (e.g., J0023+0923; Hessels et al. 2011) that do not show these effects in their radio

timing, however they have been identified as such systems based on optical follow ups of their companion, which revealed periodic modulations in the companion light curve consistent with irradiation by the pulsar wind (Breton et al. 2013). Inspection of archival data from First Generation Digitized Sky Survey (DSS-1), DSS-2, Two Micron All Sky Survey (2MASS), and *Wide-field Infrared Survey Explorer* (*WISE*) revealed no optical counterpart at the position of J0636. For comparison, if the very similar black widow system J1311−3430, which has a DM estimated distance of 1.4 kpc were at the position of J0636, its companion would have a magnitude of about 16 at maximum and 19.2 at superior conjunction.

An interesting aspect of the PSR J1719−1438 system is the large implied density of the companion ($\gtrsim 23$ g cm^{-3}). This lower limit is derived from the mean density–orbital period relation (Frank et al. 2002), which does not depend on the inclination of the system. Applying the same calculation to J0636, which has a tighter orbit and more massive companion, gives roughly a factor of two denser companion $\gtrsim 43$ g cm^{-3}. The PSR J1719−1438 formation scenario presented by Bailes et al. (2011) is that the system may have been an ultra compact X-ray binary (UCXB) system in which the companion was
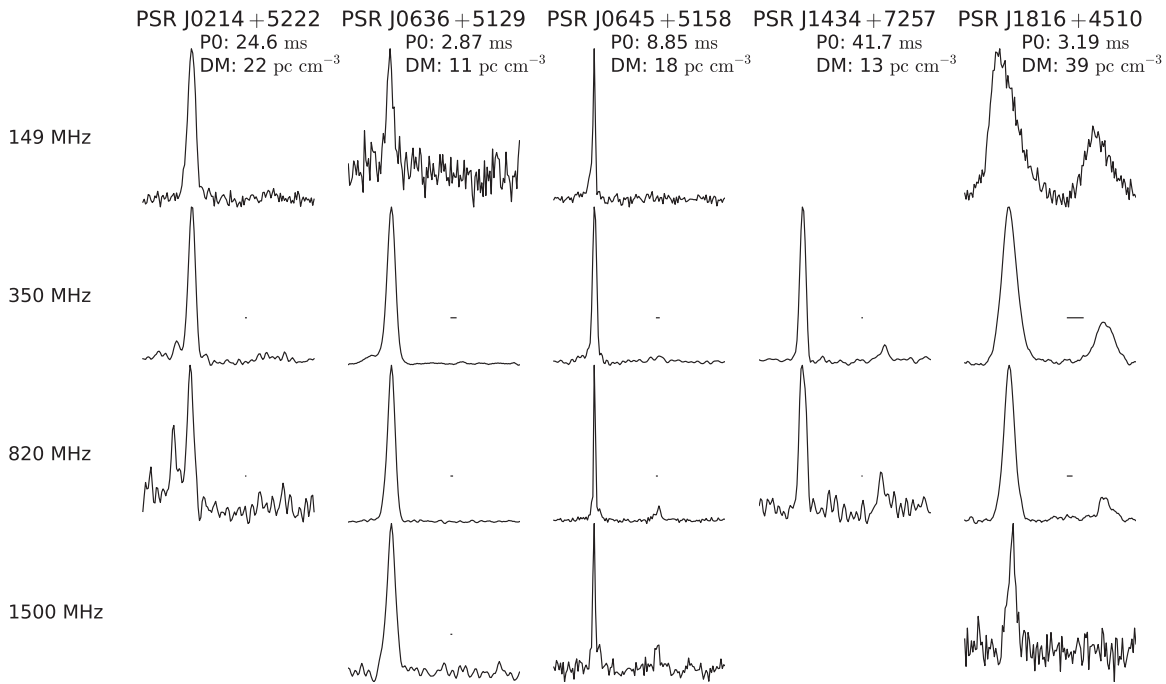
Figure 7. Pulse profiles for PSRs J0214 + 5222, J0636 + 5129, J0645 + 5158, J1434 + 7257, and J1816 + 4510 are shown. Each profile was calculated by summing profiles from multiple observations (ranging from 10 minutes to 1 hr) at the same frequency and each contains 128 phase bins. The 149 MHz profiles were made from LOFAR observations, while 350 MHz, 820 MHz, and 1500 MHz profiles were made from observations using the GBT's GUPPI backend. The 1500 MHz profile of PSR J0636 + 5129 and the profiles of all pulsars at 350 MHz and 820 MHz were created with incoherently de-dispersed data, but the 1500 MHz profiles of PSRs J0645 + 5158 and J1816 + 4510 as well as all 149 MHz profiles were created using coherently de-dispersed data. Profiles made from incoherently de-dispersed data have lines showing dispersive smearing within the frequency channels for that particular profile.

almost completely destroyed by accretion. It has been postulated that this process could be aided by some combination of a wind from the donor and/or evaporation by the pulsar wind and irradiation through X-ray feedback (van Haaften et al. 2012a; Benvenuto et al. 2012).

J0636 may have undergone a similar history and therefore may be extremely useful in characterizing such systems. We note that the orbital period and minimum companion mass of this system agrees well with the relation in Deloye & Bildsten (2003). Bailes et al. (2011) unsuccessfully attempted to detect the companion of PSR J1719−1438 using the Keck 10 m telescope down to a limit of $R \sim 24$. However, J0636 is a better candidate for optical follow up for multiple reasons. J0636 is nearby, it has high Galactic longitude ($163°9$) and latitude ($18°6$), and the companion is more massive. Such observations would help to constrain the nature (radius, temperature, and eventually composition and inclination) of the companion. This could then be combined with studies of the expected evolutionary scenarios (Deloye & Bildsten 2003; van Haaften et al. 2012b) and interior temperature to determine the history of this system and see if it is connected to UCXB systems.

In addition to being in an interesting binary system, J0636 is also a very fast-spinning, bright, nearby MSP with a small duty cycle and therefore may be a useful source for PTAs. This source has been released to the PTAs and is being tested for possible inclusion in their timing programs; it is also a good candidate for VLBI observations due to its proximity and mean flux density at 1.4 GHz.

6.3. PSR J0645 + 5158

PSR J0645 + 5158 is a bright, isolated MSP with a very small duty cycle (1%–2%) that has already been added to the timing programs of PTAs. The measured DM of 18.2 pc cm^{-3}

implies a distance of about 0.7 kpc using the NE2001 model for the Galactic electron density (Cordes & Lazio 2003). PSR J0645 + 5158 shows signs of some scintillation, which is expected given the low DM, but typically has multiple scintles within the observed bandwidth, so it is reliably detected. The observations centered at 820 MHz have provided the best timing results. The current timing solution has a residual rms of 0.51 μs, which has allowed us to measure the proper motion of J0645 + 5158 to be 7.56(25) mas yr^{-1} and an annual parallax of 1.4(3) mas. After correction for Lutz–Kelker bias, we get a parallax of 0.96(35) mas, which results in a distance measurement of $0.65^{+0.20}_{-0.13}$ kpc; this is in good agreement with the distance obtained from the NE2001 model. Using the distance of 0.65 kpc, we measure a transverse velocity for PSR J0645 + 5158 of 25 km s^{-1}. We note that we have not accounted for proper motion due to the peculiar velocity of the sun or due to differential Galactic rotation, both of which are significant compared to the measured 25 km s^{-1}.

6.4. PSR J1434 + 7257

PSR J1434 + 7257 is a partially recycled pulsar with a spin period of 41.7 ms. The timing solution indicates that it is an isolated pulsar, but its relatively low period derivative indicated a characteristic age of 1.2 Gyr. The system is likely to have been partially recycled and then disrupted. It may be the end result of a disrupted neutron star system (Hills 1983; Bhattacharya & van den Heuvel 1991). The Galactic latitude of this system ($42°2$) combined with its DM-estimated distance of 0.7 kpc gives an estimated z-height of 0.47 kpc. Though we have not yet detected a proper motion for this system, we can place an upper limit of about 30 mas yr^{-1}. Assuming the DM estimated distance, this implies an upper limit on the transverse velocity for PSR J1434 + 7257 of 100 km s^{-1}.
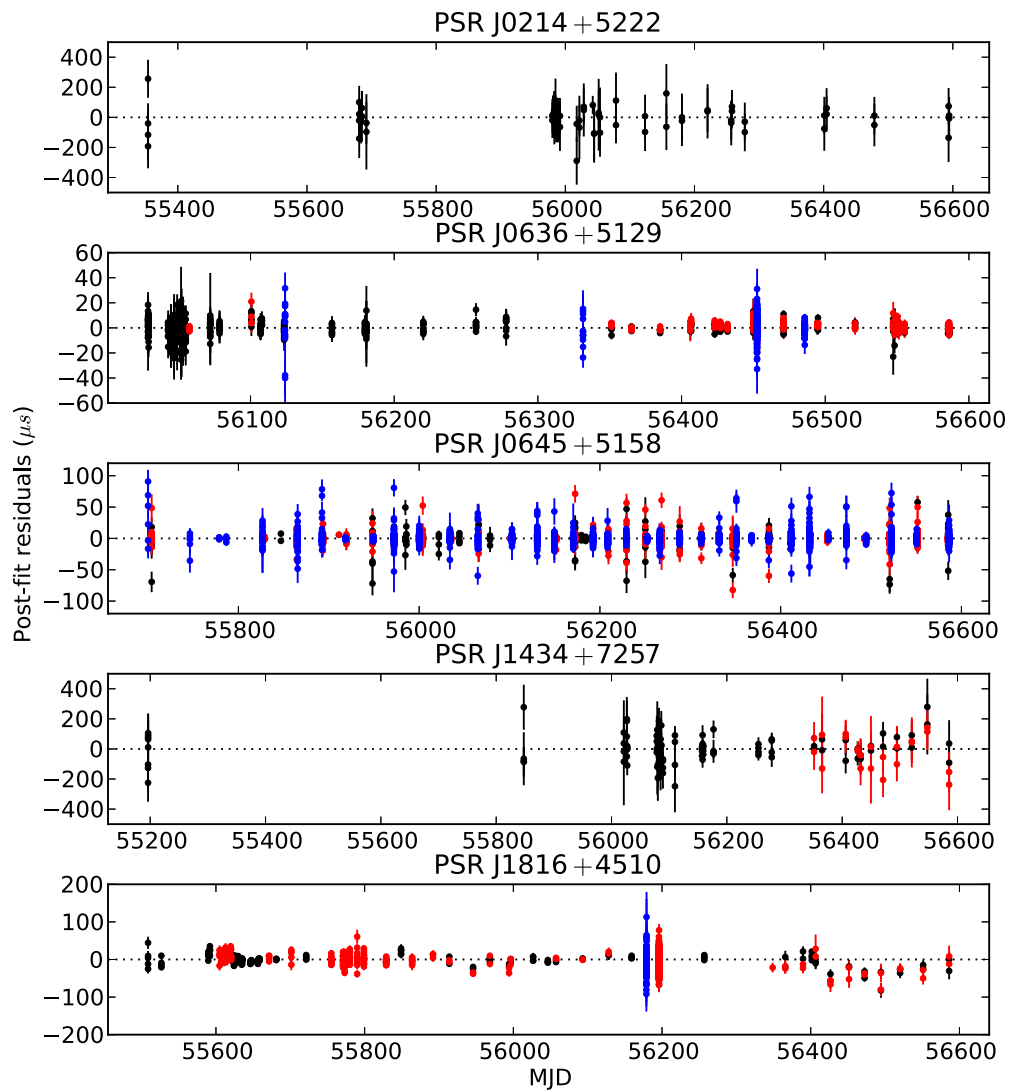
Figure 8. Post-fit residuals in microseconds for five GBNCC pulsar discoveries. Black residuals were obtained from 350 MHz observations, red residuals are from 820 MHz observations, and blue residuals were obtained from 1500 MHz observations.

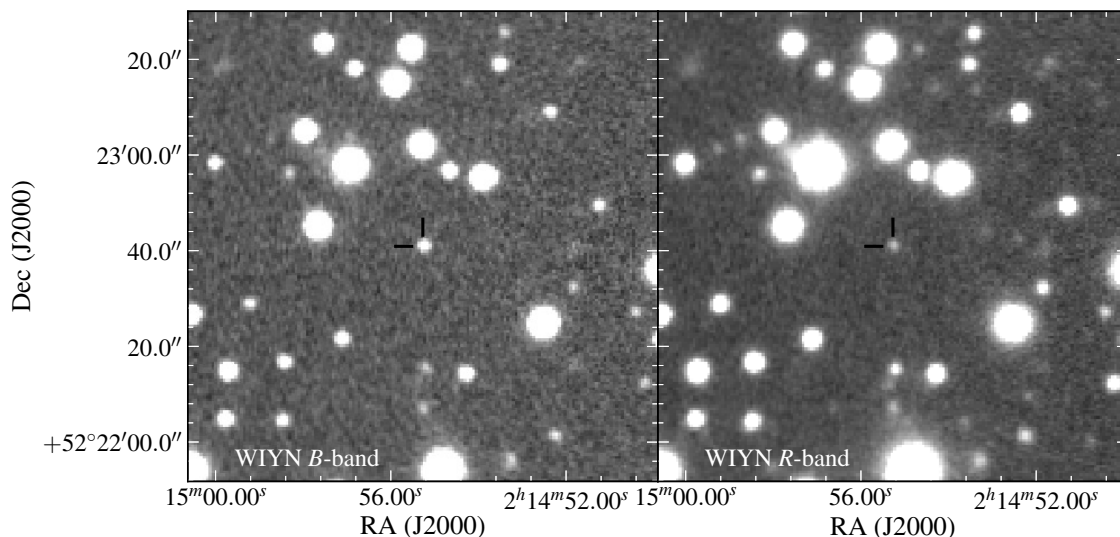(A color version of this figure is available in the online journal.)

Figure 9. Images of the field of PSR J0214+5222 from the WIYN 0.9 m telescope. The images are 1.′5 on a side. *B* band is on the left and *R* band is on the right. In each image we show ticks at the radio position of J0214+5222 that extend 2″–4″ from the pulsar. The astrometric uncertainty is far smaller, about 0.″2.
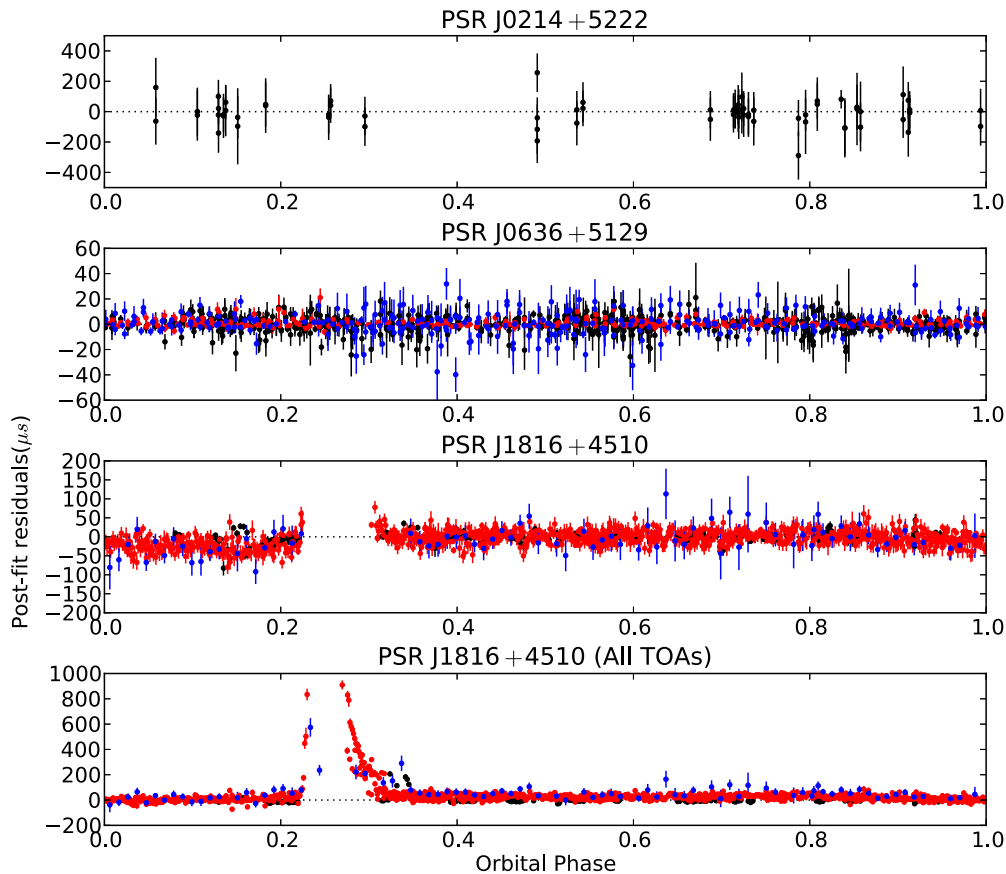
Figure 10. TOA residuals vs. orbital phase for PSRs J0214+5222, J0636+5129, and J1816+4510. The third panel shows the residuals for PSR J1816+4510 with TOAs delayed due to extra material in the system near eclipse removed. The bottom panel shows the residuals for J1816+4510 including TOAs near eclipse. Black residuals are from 350 MHz observations, red were obtained from 820 MHz observations, and blue are from 1500 MHz observations.

(A color version of this figure is available in the online journal.)

6.5. PSR J1816+4510

PSR J1816+4510 (hereafter J1816) was the source we discovered by searching beams containing a *Fermi* gamma-ray point source. This MSP was discovered in a beam coincident with the *Fermi* one yr catalog (Abdo et al. 2010) source 1FGL J1816.7+4509. Follow-up observations were performed in the weeks after discovery showing that the MSP is in an eclipsing binary system with an orbital period of 8.7 hr and a projected semi-major axis of 0.6 lt-s with very little eccentricity. Assuming a pulsar mass of 1.4 $M_\odot$, the companion has a minimum mass of 0.16 $M_\odot$ and a median predicted mass of 0.19 $M_\odot$. The length of the eclipses is approximately 7%–10% of the orbital period, which implies that the eclipsing region has a minimum diameter of 1.3 $R_\odot$. Assuming that the inclination of the system is close to 90°, the size of the Roche lobe of the companion is $R_L \approx 0.5~R_\odot$. This indicates that if the companion is filling its Roche lobe, then the diameter of the companion ($2R_L \approx 1.0~R_\odot$) is comparable to the size of the eclipsing region. Delays in pulse TOAs are seen just before and after eclipses. If we assume that these are due to an increased DM then we get an additional DM of up to 0.14 pc cm^{-3}. If we assume these electrons are constrained to a size comparable to the Roche lobe of the companion, then the electron density in this region is up to 6×10^6 cm^{-3}. The companion mass, eclipsing nature, and DM variations directly before and after eclipse initially led us to believe this source is another redback system.

After a few months of follow-up observations, we were able to construct a phase connected solution that constrained the position of J1816 to less than an arcsecond. Archival optical and infrared data were inspected and revealed that a bright star is coincident with the pulsar's position (Kaplan et al. 2012). Additional optical observations have been performed and reveal that the star seen in the archival data is the companion of J1816 (Kaplan et al. 2013) and that the companion's estimated effective temperature ($T_{\rm eff}$) is about 15,000 K. This temperature is significantly greater than $T_{\rm eff}$ for any known redback system ($T_{\rm eff} \lesssim 6000$ K). Also, the spectroscopic study performed by Kaplan et al. (2013) showed strong lines of helium and metals. J1816 seems to have several properties that make it distinct among the eclipsing pulsar systems.

J1816 was observed by the *Chandra X-Ray Observatory* for 33.5 ks, which is slightly longer than one orbital period, using the ACIS-S detector on 2013 July 22. The data were analyzed using CIAO[30] version 4.5 and Xspec[31] version 12.8. A total of 17 photons were detected between 0.3 and 8 keV in a 2″ radius region centered on the timing position of the pulsar, with likely no more than two being background photons. One of the photons had an energy of around 4 keV, and four in the 1.5–2 keV range, suggesting some of the emission could be non-thermal, given the typical temperatures of thermal emission from MSPs are in a fairly narrow range of 0.15–0.2 keV (e.g., Zhang & Cheng

---

[30] http://cxc.cfa.harvard.edu/ciao/
[31] http://heasarc.nasa.gov/xanadu/xspec/

2003; Bogdanov et al. 2007, 2008). However, it is likely that the thermal emission dominates as is the case for most MSPs. The total 0.3–8 keV flux was $4.3 \pm 1.1 \times 10^{-15}$ erg cm^{-2} s^{-1}, assuming a model with $kT = 0.17$ keV, $nH = 0.02 \times 10^{20}$ cm^{-2}, and using a power-law index of 1.5. Given the high Galactic latitude and distance estimated from either the DM or optical studies, the total X-ray absorption is expected (e.g., using the HEASARC nH tool based on Dickey & Lockman (1990)) to be $nH < 3.8 \times 10^{20}$ cm^{-2}, which is quite low and so the unabsorbed flux is likely no more than 15% greater than the observed flux. Even given the larger distance estimated by Kaplan et al. (2013) of 4.5 kpc, the total X-ray luminosity is only $0.0002\dot{E}$, where $\dot{E}$ is the spindown luminosity given in Table 4. This is typical for ordinary MSPs suggesting there is very little X-ray emission arising from an intrabinary shock, unlike what is seen from most redbacks (Roberts et al. 2014).

7. CONCLUSIONS

The GBNCC is a 350 MHz pulsar and fast transient survey of the entire sky visible by the GBT. Our sensitivity is about 2.5 times better than previous surveys for regions of the sky not visible by the Arecibo Observatory. In the Arecibo visible range ($-2° > \delta > 38°$), we have comparable sensitivity to previous surveys for normal pulsars and much better sensitivity to MSPs. As of 2014 March 18, we have completed observations for about 35% of the full survey and have analyzed about 75% of the data recorded thus far. Using previously known pulsars detected in our survey, we have compared expected survey sensitivity to actual sensitivity and conclude that the results roughly agree. We have provided parameters for these re-detections (as well as for our new discoveries), which will be useful for future pulsar population models.

To date, our survey has resulted in the discovery of 67 new radio pulsars, whose parameters were reported here, as well as 7 new RRATs. Of the 67 new pulsars, 9 of them are MSPs. Comparison of the 11 MSPs detected so far (9 new and 2 previously known) to the 30 MSPs expected for stage 1 from simulations suggest that there are still more discoveries to be made. We note that about 20% of the stage 1 data remains to be processed and that of the 80% that has been processed, we have performed only a cursory examination of a large fraction of the candidates. We estimate that the candidates have been examined at roughly the 50% level, so additional discoveries are likely in stage 1 data. A major issue for large-scale pulsar surveys such as the GBNCC is the difficulty in examining all of the candidates. We have used computer algorithms to generate scores for each candidate and increased the number of people looking through the candidates by teaching high school and undergraduate students to identify potential pulsar signals. These students have examined over 200,000 candidates and are responsible for the discovery of roughly 50 new pulsars in the GBNCC survey.

We have reported discovery parameters for 62 of our discovered pulsars and timing solutions for five more pulsars, including two short-period binary MSPs (PSRs J0636 + 5129 and J1816 + 4510), a long-period binary MSP (PSR J0214 + 5222), an isolated MSP (PSR J0645 + 5158), and an isolated, partially recycled pulsar (PSR J1434 + 7257). PSR J0636 + 5129 has orbital and companion mass parameters that are very similar to black widow pulsar systems, however it does not show any evidence of the companion being ablated. It may instead be more similar to the diamond planet pulsar systems. PSR J1816 + 4510 is an eclipsing binary system with an orbital period and

Table 5
Offset from GBNCC Beam Center and the Estimated Flux Densities for 64 Re-detections of 55 Known Pulsars Detected in the GBNCC Survey

Pulsar	r (°)	S_{350}^{o} (mJy)
B0037+56	0.21	5.0
B0037+56	0.30	4.7
B0059+65	0.24	29.7
B0105+68	0.19	30.5
B0114+58	0.30	43.4
B0136+57	0.15	52.7
B0138+59	0.25	64.9
B0154+61	0.16	7.3
J0215+6218	0.27	14.5
J0215+6218	0.28	17.2
J0218+4232	0.26	57.7
J0218+4232	0.29	39.8
B0226+70	0.24	40.0
B0320+39	0.13	10.8
J0341+5711	0.15[a]	364.7
B0353+52	0.10	21.6
B0355+54	0.21	46.8
B0410+69	0.05	6.7
B0450+55	0.15	49.9
B0458+46	0.08	10.9
B0609+37	0.30	8.8
B0643+80	0.13	6.1
B0655+64	0.20	10.1
B0809+74	0.12	41.1
B0841+80	0.06	9.0
B1112+50	0.26	5.3
B1112+50	0.27	5.2
B1322+83	0.25	22.4
B1322+83	0.26	14.1
B1508+55	0.18	39.3
J1518+4904	0.22	3.4
B1839+56	0.16	57.9
B1946+35	0.09	108.5
B2000+40	0.30	4.7
J2027+4557	0.06	14.2
B2027+37	0.16	31.2
B2035+36	0.20	12.6
J2043+7045	0.28[a]	63.7
B2045+56	0.17	18.5
B2053+36	0.27	37.5
B2106+44	0.28	37.0
B2111+46	0.18	47.2
J2217+5733	0.18	2.8
J2217+5733	0.18	4.6
B2217+47	0.29	42.0
J2222+5602	0.22[a]	21.1
B2224+65	0.22	35.4

Table 5
(Continued)

Pulsar	r (°)	S^o_{350} (mJy)
J2229+6114	0.13	1.5
B2227+61	0.17	24.9
J2238+6021	0.16[a]	111.1
B2241+69	0.19	6.3
B2241+69	0.19	6.6
B2255+58	0.10	251.9
J2302+6028	0.11	36.0
J2302+4442	0.11	11.3
B2306+55	0.25	122.2
B2306+55	0.26	53.0
B2310+42	0.15	7.3
B2319+60	0.17	303.2
B2323+63	0.20	42.2
B2324+60	0.11	26.9
B2324+60	0.11	27.7
J2352+65	0.27[a]	26.5
B2351+61	0.24	15.1

Note. [a] The position of these pulsars obtained from the ATNF database are only to the nearest 0°.25.

companion mass resembling redback pulsar systems, however optical follow up has indicated that the companion is quite unlike typical redback systems and may be young and that this system has recently completed its spin-up phase. PSR J0214+5222 is a partially recycled MSP in a long-period orbit with a 0.4 $M_\odot$ companion. Comparison to archival optical catalogs revealed an optical counterpart at the position of J0214+5222 that is brighter than would be expected for typical pulsar systems with a white dwarf companion. The companion may either be a very young white dwarf, or instead could be a subdwarf B star, making this the first known PSR-sdB system. Two of our discoveries (PSR J0636+5129 and PSR J0645+5158) are bright, low-DM MSPs that are likely to be useful in efforts to detect GWs using PTAs.

Facilities: GBT, WIYN:0.9m (S2KB), *CXO*

APPENDIX

Table 5 contains 64 observations of 55 previously known pulsars that have thus far been re-detected in the GBNCC survey within the 18′ HWHM of the 350 MHz GBT beam. The period and DM as detected by the GBNCC survey are given, as well as the distance from the center of the beam in which the pulsar was detected, and the observed mean flux density at 350 MHz (for a description, see Section 4).

REFERENCES

Abdo, A. A., Ackermann, M., Ajello, M., et al. 2010, yCat, 218, 80405
Antoniadis, J., Freire, P. C. C., Wex, N., et al. 2013, Sci, 340, 448
Archibald, A. M., Stairs, I. H., Ransom, S. M., et al. 2009, Sci, 324, 1411
Bailes, M., Bates, S. D., Bhalerao, V., et al. 2011, Sci, 333, 1717
Barr, E. D., Champion, D. J., Kramer, M., et al. 2013, MNRAS, 435, 2234
Bates, S. D., Lorimer, D. R., & Verbiest, J. P. W. 2013, MNRAS, 431, 1352
Benvenuto, O. G., De Vito, M. A., & Horvath, J. E. 2012, ApJL, 753, L33
Bergeron, P., Wesemael, F., Dufour, P., et al. 2011, ApJ, 737, 28
Bertin, E., & Arnouts, S. 1996, A&AS, 117, 393
Bhattacharya, D., & van den Heuvel, E. P. J. 1991, PhR, 203, 1
Biggs, J. D., Bailes, M., Lyne, A. G., Goss, W. M., & Fruchter, A. S. 1994, MNRAS, 267, 125
Blandford, R., & Teukolsky, S. A. 1976, ApJ, 205, 580
Bogdanov, S., Grindlay, J. E., & Rybicki, G. B. 2008, ApJ, 689, 407
Bogdanov, S., Rybicki, G. B., & Grindlay, J. E. 2007, ApJ, 670, 668
Boyles, J., Lynch, R. S., Ransom, S. M., et al. 2013, ApJ, 763, 80
Breton, R. P., van Kerkwijk, M. H., Roberts, M. S. E., et al. 2013, ApJ, 769, 108
Burgay, M., D'Amico, N., Possenti, A., et al. 2003, Natur, 426, 531
Camilo, F. 2003, in ASP Conf. Ser. 302, Radio Pulsars, ed. M. Bailes, D. J. Nice, & S. E. Thorsett (San Francisco, CA: ASP), 145
Champion, D. J., Ransom, S. M., Lazarus, P., et al. 2008, Sci, 320, 1309
Coenen, T., van Leeuwen, J., & Stairs, I. H. 2011, A&A, 531, A125
Cognard, I., Guillemot, L., Johnson, T. J., et al. 2011, ApJ, 732, 47
Cordes, J. M. 2002, in ASP Conf. Ser. 278, Single-Dish Radio Astronomy: Techniques and Applications, ed. S. Stanimirovic, D. Altschuler, P. Goldsmith, & C. Salter (San Francisco, CA: ASP), 227
Cordes, J. M., Freire, P. C. C., Lorimer, D. R., et al. 2006, ApJ, 637, 446
Cordes, J. M., & Lazio, T. J. W. 2002, arXiv:astro-ph/0207156
Cordes, J. M., & Lazio, T. J. W. 2003, arXiv:astro-ph/0301598
D'Amico, N., Lyne, A. G., Manchester, R. N., Possenti, A., & Camilo, F. 2001, ApJL, 548, L171
Deloye, C. J., & Bildsten, L. 2003, ApJ, 598, 1217
Demorest, P. B., Ferdman, R. D., Gonzalez, M. E., et al. 2013, ApJ, 762, 94
Demorest, P. B., Pennucci, T., Ransom, S. M., Roberts, M. S. E., & Hessels, J. W. T. 2010, Natur, 467, 1081
Deneva, J. S., Stovall, K., McLaughlin, M. A., et al. 2013, ApJ, 775, 51
Dewey, R. J., Taylor, J. H., Weisberg, J. M., & Stokes, G. H. 1985, ApJL, 294, L25
Dickey, J. M., & Lockman, F. J. 1990, ARA&A, 28, 215
Drimmel, R., Cabrera-Lavers, A., & López-Corredoira, M. 2003, A&A, 409, 205

---

[32] http://www.tacc.utexas.edu

Frank, J., King, A., & Raine, D. 2002, in Accretion Power in Astrophysics (3rd ed.; Cambridge Univ. Press)
Freire, P. C. C., Wex, N., Esposito-Farèse, G., et al. 2012, MNRAS, 423, 3328
Fruchter, A. S., Stinebring, D. R., & Taylor, J. H. 1988, Natur, 333, 237
Gavriil, F. P., Gonzalez, M. E., Gotthelf, E. V., et al. 2008, Sci, 319, 1802
Guillemot, L., Freire, P. C. C., Cognard, I., et al. 2012, MNRAS, 422, 1294
Haslam, C. G. T., Salter, C. J., Stoffel, H., & Wilson, W. E. 1982, A&AS, 47, 1
Heber, U. 2009, ARA&A, 47, 211
Hessels, J. W. T., Ransom, S. M., Stairs, I. H., Kaspi, V. M., & Freire, P. C. C. 2007, ApJ, 670, 363
Hessels, J. W. T., Ransom, S. M., Stairs, I. H., et al. 2006, Sci, 311, 1901
Hessels, J. W. T., Roberts, M. S. E., McLaughlin, M. A., et al. 2011, in AIP Conf. Ser. 1357, ed. M. Burgay, N. D'Amico, P. Esposito, A. Pellizzoni, & A. Possenti (Melville, NY: AIP), 40
Hewish, A., Bell, S. J., Pilkington, J. D. H., Scott, P. F., & Collins, R. A. 1968, Natur, 217, 709
Hills, J. G. 1983, ApJ, 267, 322
Hulse, R. A., & Taylor, J. H. 1975, ApJL, 195, L51
Johnston, S., Manchester, R. N., Lyne, A. G., et al. 1992, ApJL, 387, L37
Kaplan, D. L., Bhalerao, V. B., van Kerkwijk, M. H., et al. 2013, ApJ, 765, 158
Kaplan, D. L., Escoffier, R. P., Lacasse, R. J., et al. 2005, PASP, 117, 643
Kaplan, D. L., Stovall, K., Ransom, S. M., et al. 2012, ApJ, 753, 174
Kaplan, D. L., van Kerkwijk, M. H., Koester, D., et al. 2014, ApJL, 783, L23
Kaspi, V. M., Johnston, S., Bell, J. F., et al. 1994, ApJL, 423, L43
Keith, M. J., Jameson, A., van Straten, W., et al. 2010, MNRAS, 409, 619
Keith, M. J., Johnston, S., Ray, P. S., et al. 2011, MNRAS, 414, 1292
Kerr, M., Camilo, F., Johnson, T. J., et al. 2012, ApJL, 748, L2
Kramer, M., Stairs, I. H., Manchester, R. N., et al. 2006, Sci, 314, 97
Lange, C., Camilo, F., Wex, N., et al. 2001, MNRAS, 326, 274
Lazarus, P. 2013, in IAU Symp. 291, Neutron Stars and Pulsars: Challenges and Opportunities after 80 years, ed. J. van Leeuwen (Cambridge: Cambridge Univ. Press), 35
Lee, K. J., Stovall, K., Jenet, F. A., et al. 2013, MNRAS, 433, 688
Lorimer, D. R. 2013, in IAU Symp. 291, Neutron Stars and Pulsars: Challenges and Opportunities after 80 years, ed. J. van Leeuwen (Cambridge: Cambridge Univ. Press), 237
Lorimer, D. R., Bailes, M., McLaughlin, M. A., Narkevic, D. J., & Crawford, F. 2007, Sci, 318, 777
Lynch, R. S., Boyles, J., Ransom, S. M., et al. 2013, ApJ, 763, 81
Manchester, R. N., Hobbs, G., Bailes, M., et al. 2013, PASA, 30, e017
Manchester, R. N., Lyne, A. G., Camilo, F., et al. 2001, MNRAS, 328, 17
Manchester, R. N., Lyne, A. G., Robinson, C., Bailes, M., & D'Amico, N. 1991, Natur, 352, 219

McLaughlin, M. A., Lyne, A. G., Lorimer, D. R., et al. 2006, Natur, 439, 817
Ng, C. 2013, in IAU Symp. 291, Neutron Stars and Pulsars: Challenges and Opportunities after 80 years, ed. J. van Leeuwen (Cambridge: Cambridge Univ. Press), 53
Papitto, A., Ferrigno, C., Bozzo, E., et al. 2013, Natur, 501, 517
Pletsch, H. J., Guillemot, L., Fehrmann, H., et al. 2012, Sci, 338, 1314
Ransom, S. M. 2001, PhD thesis, Harvard Univ.
Ransom, S. M., Eikenberry, S. S., & Middleditch, J. 2002, AJ, 124, 1788
Ransom, S. M., Hessels, J. W. T., Stairs, I. H., et al. 2005, Sci, 307, 892
Ransom, S. M., Ray, P. S., Camilo, F., et al. 2011, ApJL, 727, L16
Ransom, S. M., Stairs, I. H., Archibald, A. M., et al. 2014, Natur, 505, 520
Ray, P. S., Ransom, S. M., Cheung, C. C., et al. 2013, ApJL, 763, L13
Roberts, M. S. E. 2011, in AIP Conf. Ser. 1357, Radio Pulsars: An Astrophysical Key to Unlock the Secrets of the Universe, ed. M. Burgay, N. D'Amico, P. Esposito, A. Pellizzoni, & A. Possenti (San Francisco, CA: ASP), 127
Roberts, M. S. E., Mclaughlin, M. A., Gentile, P., et al. 2014, AN, 335, 313
Romani, R. W., Filippenko, A. V., Silverman, J. M., et al. 2012, ApJL, 760, L36
Saff, E., & Kuijlaars, A. 1997, The Mathematical Intelligencer, 19, 5
Shklovskii, I. S. 1970, SvA, 13, 562
Stappers, B. W., Hessels, J. W. T., Alexov, A., et al. 2011, A&A, 530, A80
Stetson, P. B. 2000, PASP, 112, 925
Tauris, T. M., Langer, N., & Kramer, M. 2012, MNRAS, 425, 1601
Tauris, T. M., & Savonije, G. J. 1999, A&A, 350, 928
Taylor, J. H. 1992, RSPTA, 341, 117
Taylor, J. H., & Weisberg, J. M. 1989, ApJ, 345, 434
Thornton, D., Stappers, B., Bailes, M., et al. 2013, Sci, 341, 53
Tremblay, P.-E., Bergeron, P., & Gianninas, A. 2011, ApJ, 730, 128
van Haaften, L. M., Nelemans, G., Voss, R., & Jonker, P. G. 2012a, A&A, 541, A22
van Haaften, L. M., Nelemans, G., Voss, R., Wood, M. A., & Kuijpers, J. 2012b, A&A, 537, A104
van Haarlem, M. P., Wise, M. W., Gunst, A. W., et al. 2013, A&A, 556, A2
van Haasteren, R., Levin, Y., Janssen, G. H., et al. 2011, MNRAS, 414, 3117
van Kerkwijk, M. H., Bassa, C. G., Jacoby, B. A., & Jonker, P. G. 2005, in ASP Conf. Ser. 328, Binary Radio Pulsars, ed. F. A. Rasio & I. H. Stairs (San Francisco, CA: ASP), 357
Verbiest, J. P. W., Lorimer, D. R., & McLaughlin, M. A. 2010, MNRAS, 405, 564
Wolszczan, A., & Frail, D. A. 1992, Natur, 355, 145
Zacharias, N., Finch, C., Girard, T., et al. 2009, yCat, 1315, 0
Zhang, L., & Cheng, K. S. 2003, A&A, 398, 639
Zhu, W. W., Berndsen, A., Madsen, E. C., et al. 2014, ApJ, 781, 117